Radboud Universiteit

GRAPHENE FLAGSHIP

Semiclassical dynamics of charge carriers in graphene

Mikhail Katsnelson

In collaboration with Koen Reijnders, Timur Tudorovskiy, Sergey Dobrokhotov, Dima Minenkov, and Victor Kleptsyn

Carbon, an elemental solid

Diamond

Graphite

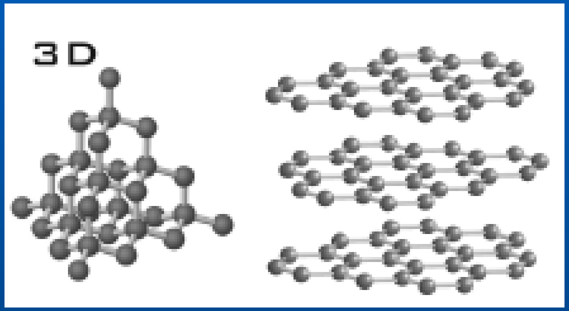

Crystal lattices

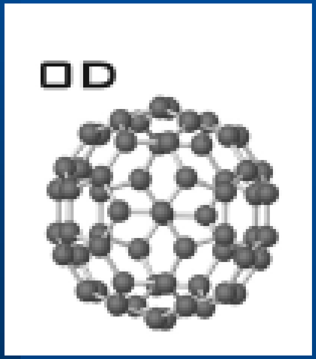

Fullerenes

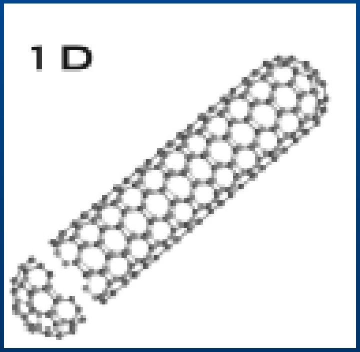

Nanotubes

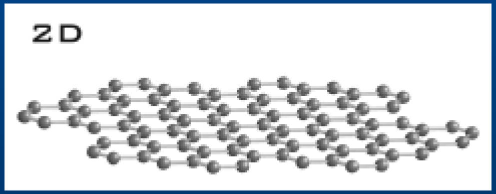

Graphene

Mother of all graphitic forms

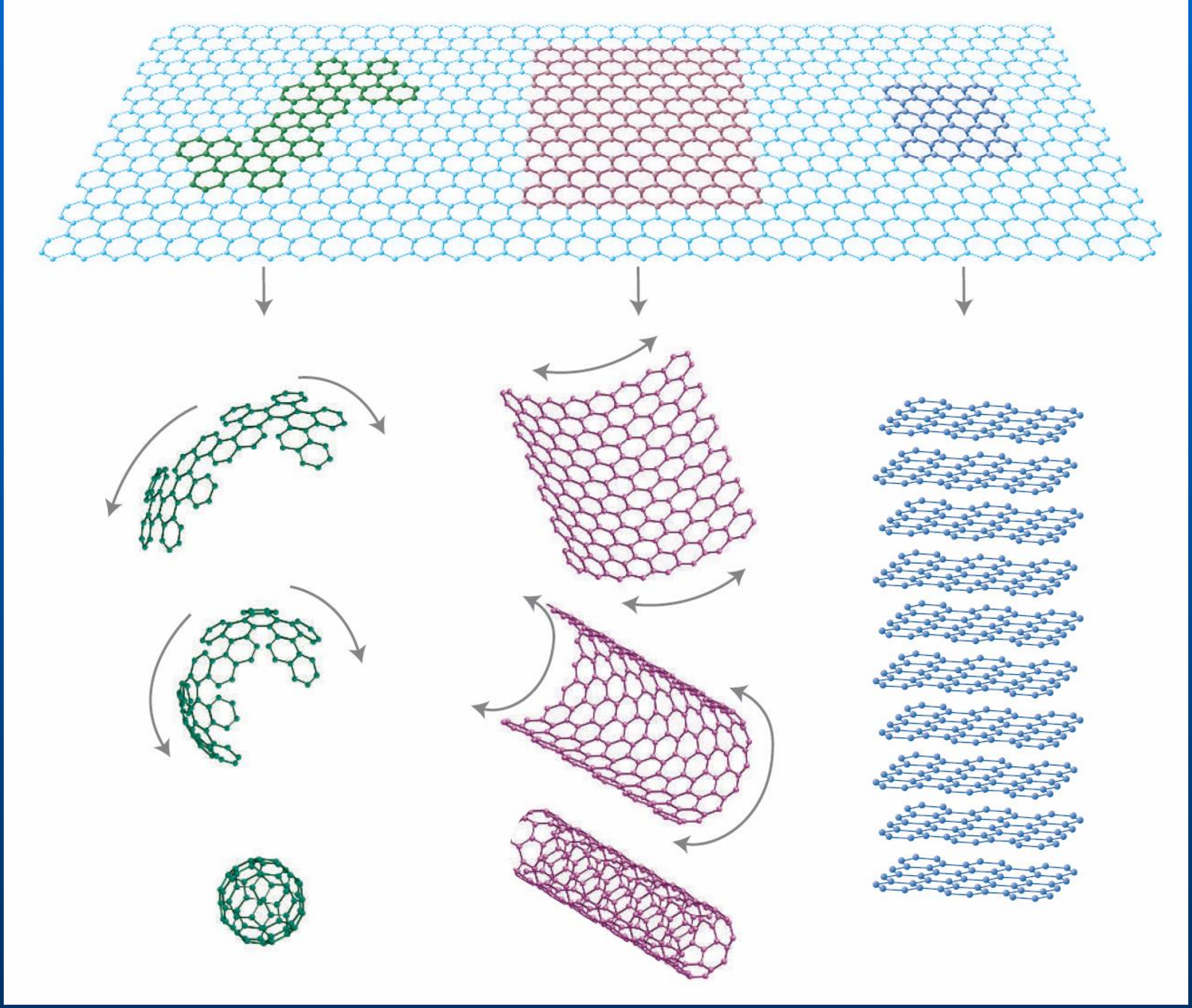

Fullerenes   Nanotubes   Graphite

Honeycomb lattice (graphene)

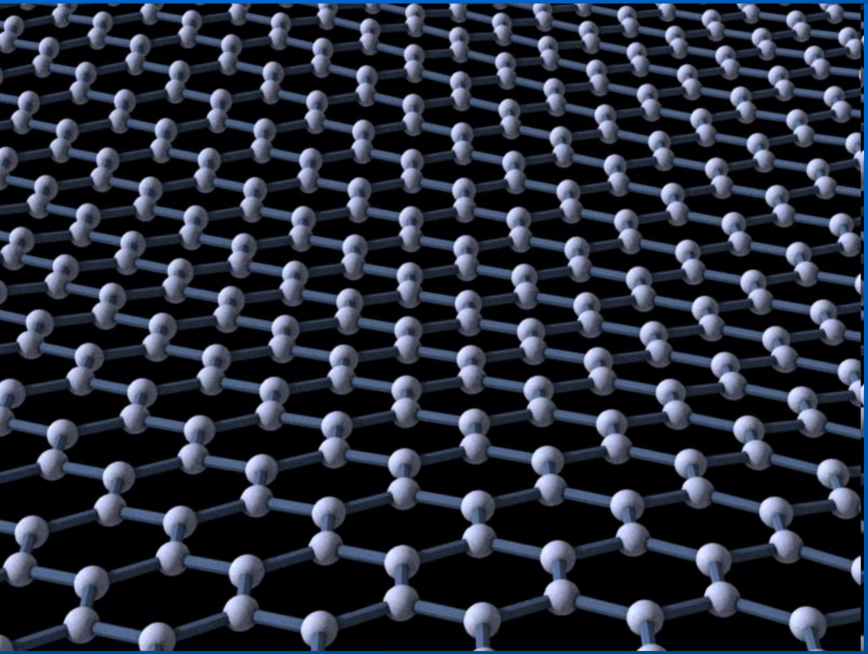

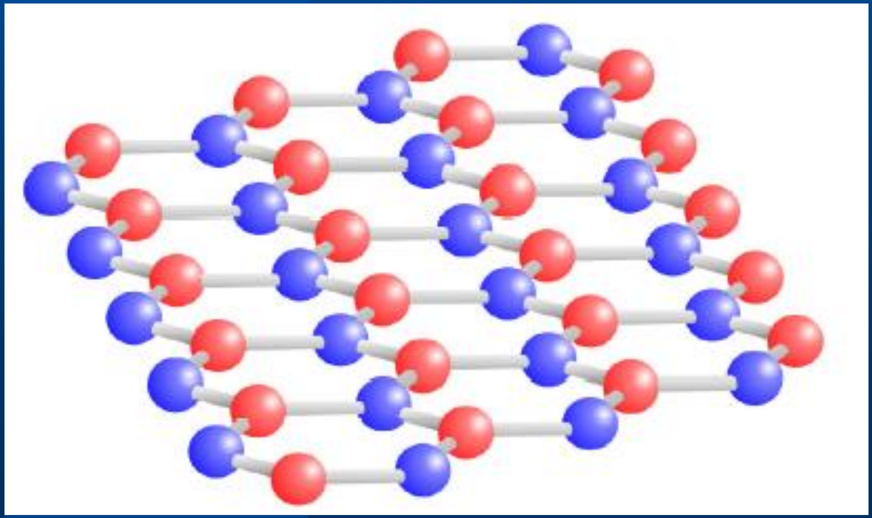

Two equivalent sublattices,
A and B (pseudospin)

Massless Dirac fermions in graphene

$$H = -i\hbar c^{*} \begin{pmatrix} 0 & \dfrac{\partial}{\partial x} - i\dfrac{\partial}{\partial y} \\ \dfrac{\partial}{\partial x} + i\dfrac{\partial}{\partial y} & 0 \end{pmatrix} \qquad \hbar c^{*} = \frac{\sqrt{3}}{2}\gamma_0 a$$

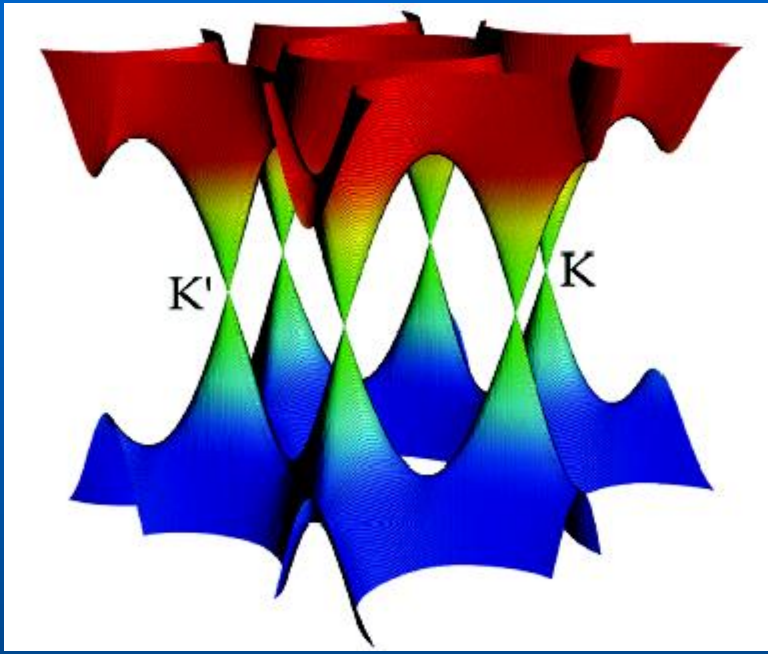

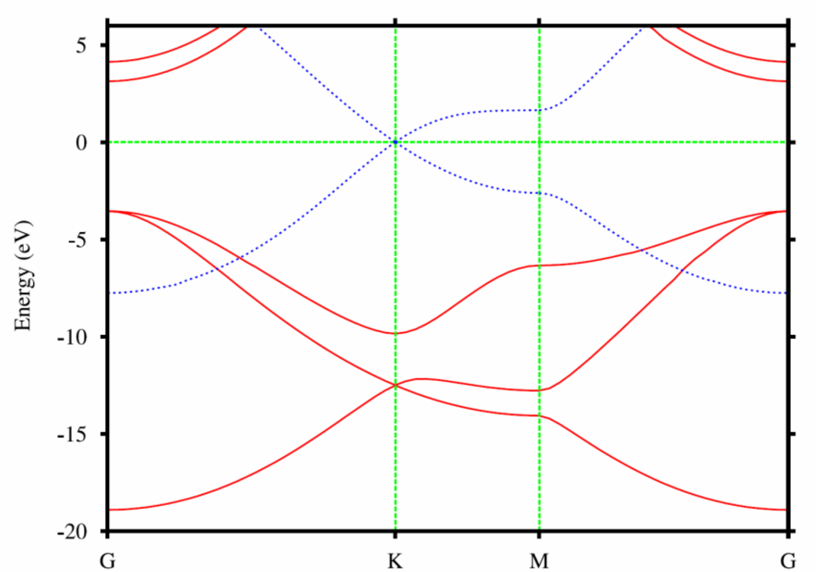

FIG. 2: (color online) Band structure of a single graphene layer. Solid red lines are σ bands and dotted blue lines are π bands.

sp^2 hybridization, π bands crossing the neutrality point

Neglecting intervalley scattering: massless Dirac fermions

Symmetry protected (*T* and *I*)

Massless Dirac fermions in condensed matter physics

1. d-wave superconductors
2. Vortices in superconductors and in superfluid helium-3
3. Topological insulators
4. Graphene

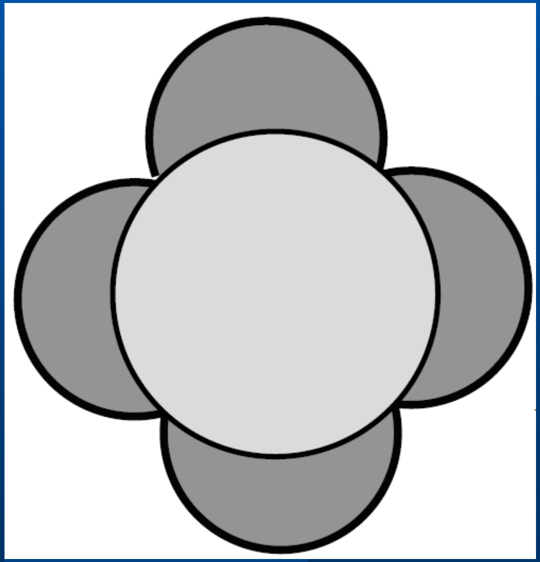

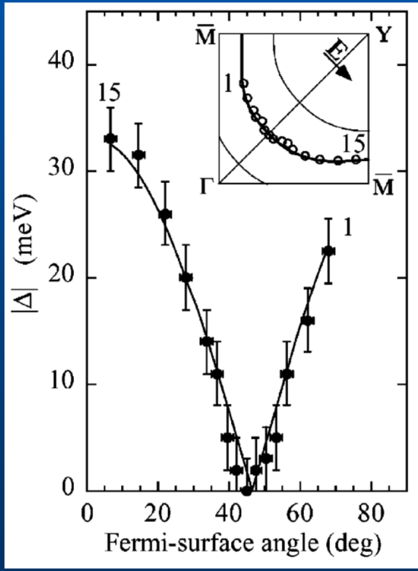

Gap in high-Tc cuprates

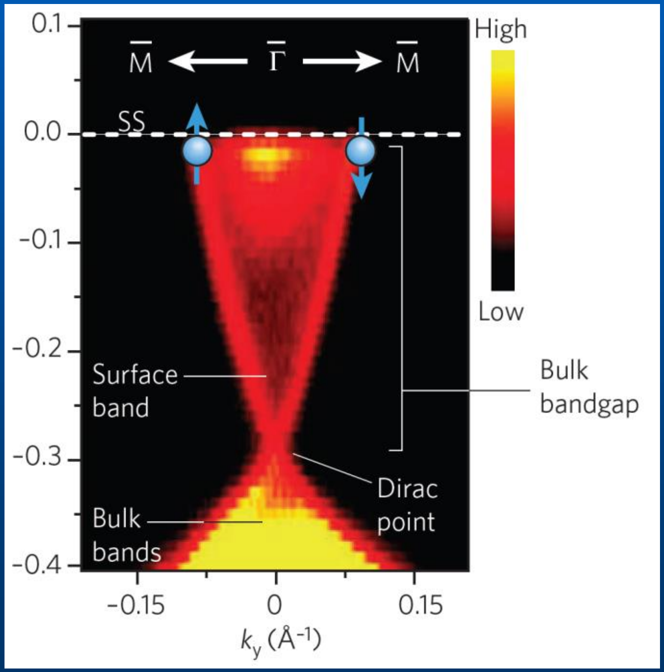

Electronic structure on surface of Bi_2Se_3

Outline

1.Chiral tunneling
Tudorovkiy, Reijnders, MIK, Phys. Scr. T 146, 014010 (2012);
Reijnders, Tudorovskiy, MIK, Ann. Phys. (NY) (2013)

2.Electron Veselago lenses and caustics
Reijnders, MIK, Phys. Rev. B 95, 115310 (2017);
Reijnders, MIK, Phys. Rev. B 96, 045305 (2017);

3.Electron optics in 2D case
Reijnders, Minenkov, MIK, Dobrokhotov, Ann. Phys.(NY) 397, 65 (2018)

4.Chiral tunneling in bilayer graphene
Kleptsyn, Okunev, Schurov, Zubov, MIK, Phys. Rev. B **92**, 165407 (2015)

See also Koen Reijnders thesis (Nijmegen, 2019)
Semiclassical dynamics of charge carriers in graphene
https://repository.ubn.ru.nl/handle/2066/204183

Chiral tunneling and Klein paradox

MIK, Novoselov, Geim, Nat. Phys. 2, 620 (2006)

Electronics: heterostructures (*p*-*n*-*p* junctions etc.)

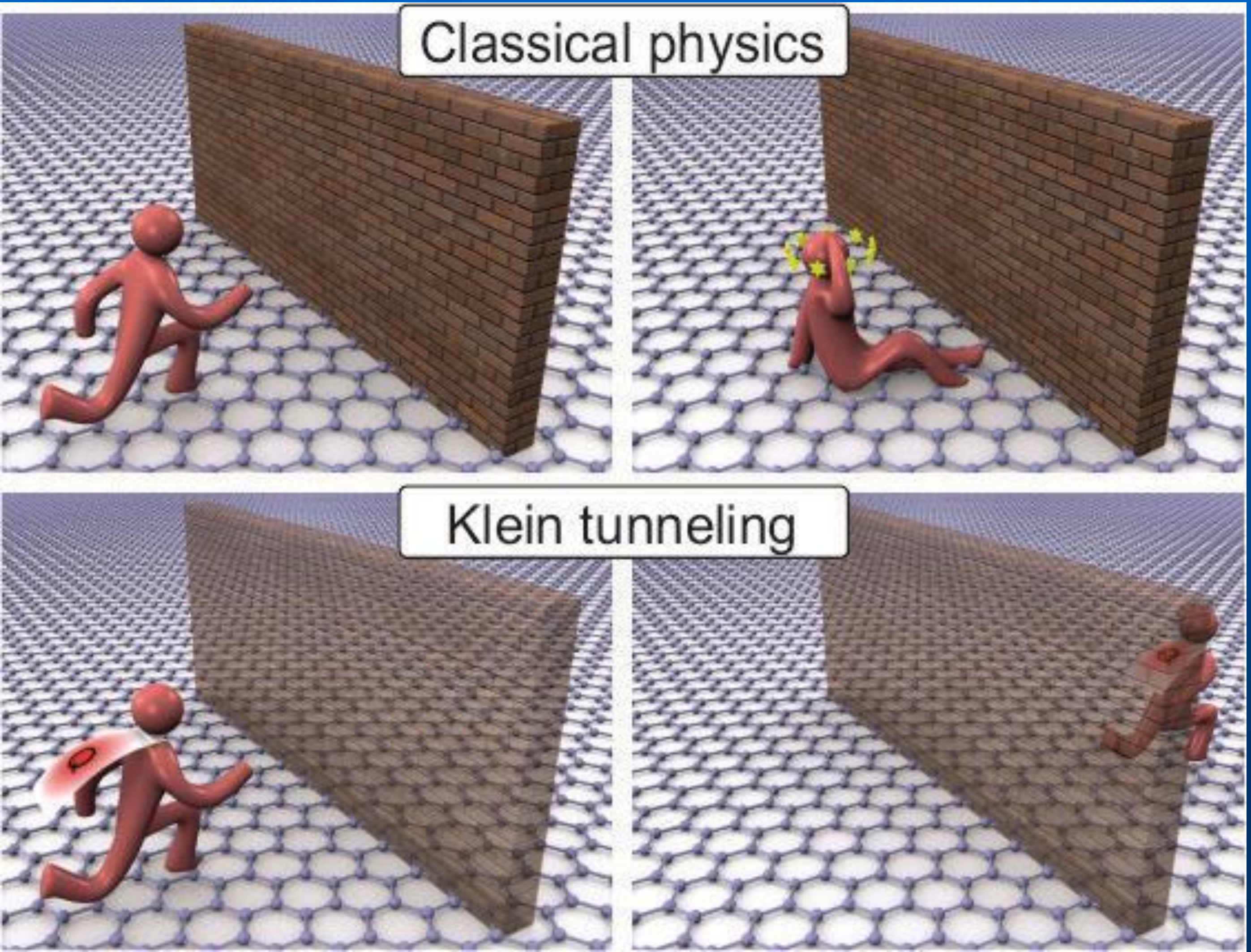

(C) Florian Sterl

Klein paradox II

Ultrarelativisic

Nonrelativistic

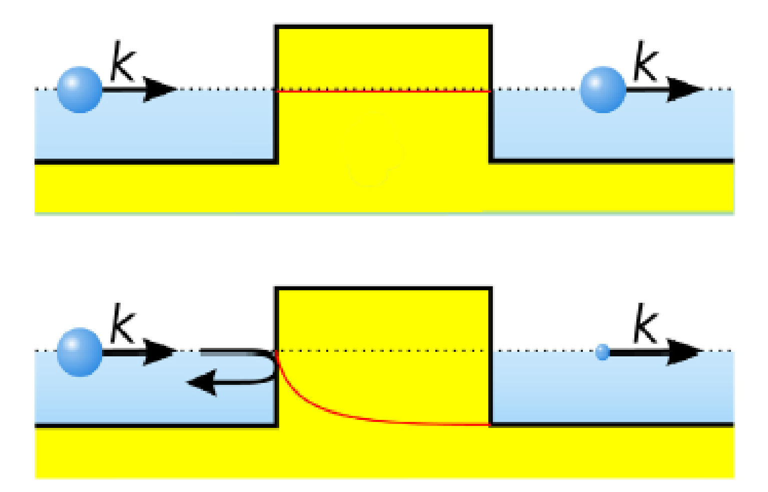

Tunnel effect: momentum and coordinate are complementary variables, kinetic and potential energy are not measurable simultaneously

Relativistic case: even the *coordinate itself* is not measurable, particle-antiparticle pair creation

Klein paradox III

Transmission probability

Barrier width 100 *nm*

Electron concentration outside barrier 0.5×10^{12} cm^{-2}

Hole concentration inside barrier 1×10^{12} cm^{-2} (red) and 3×10^{12} cm^{-2} (blue)

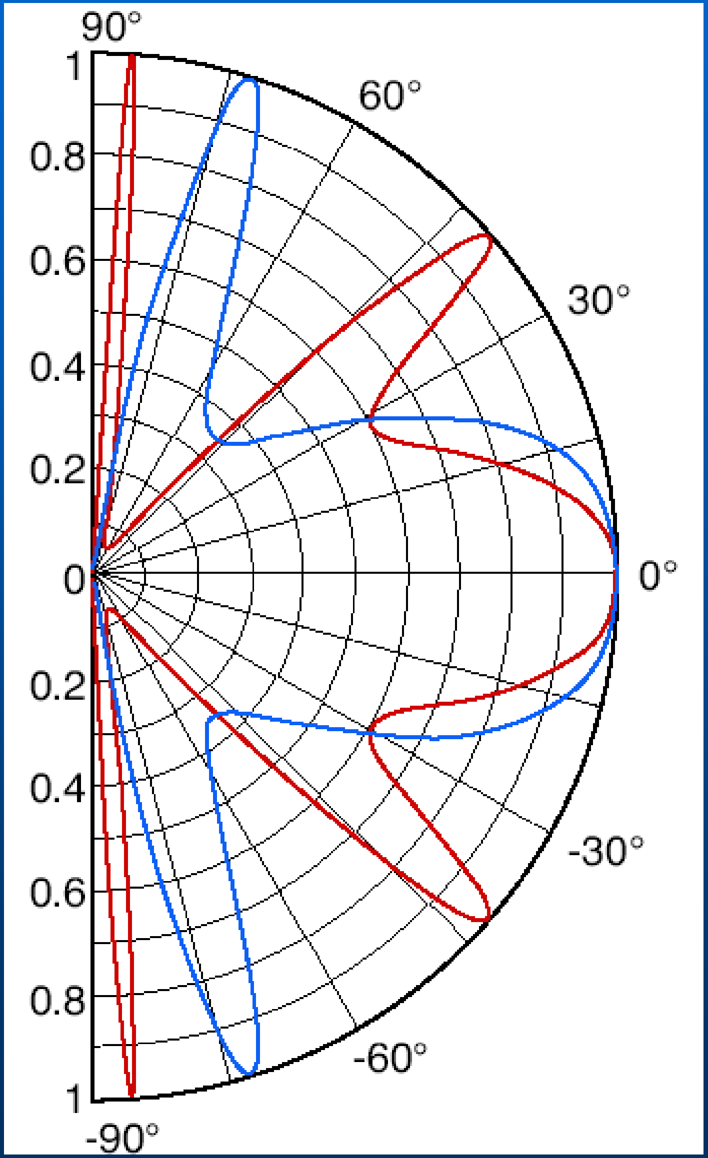

Klein tunneling: Experimental confirmation

PRL **102,** 026807 (2009) PHYSICAL REVIEW LETTERS week ending 16 JANUARY 2009

Evidence for Klein Tunneling in Graphene *p*-*n* Junctions

N. Stander, B. Huard, and D. Goldhaber-Gordon*
Department of Physics, Stanford University, Stanford, California 94305, USA
(Received 13 June 2008; published 16 January 2009)

Transport through potential barriers in graphene is investigated using a set of metallic gates capacitively coupled to graphene to modulate the potential landscape. When a gate-induced potential step is steep enough, disorder becomes less important and the resistance across the step is in quantitative agreement with predictions of Klein tunneling of Dirac fermions up to a small correction. We also perform magnetoresistance measurements at low magnetic fields and compare them to recent predictions.

nature physics
LETTERS
PUBLISHED ONLINE: 1 FEBRUARY 2009 | DOI: 10.1038/NPHYS1198

Quantum interference and Klein tunnelling in graphene heterojunctions

Andrea F. Young and Philip Kim*

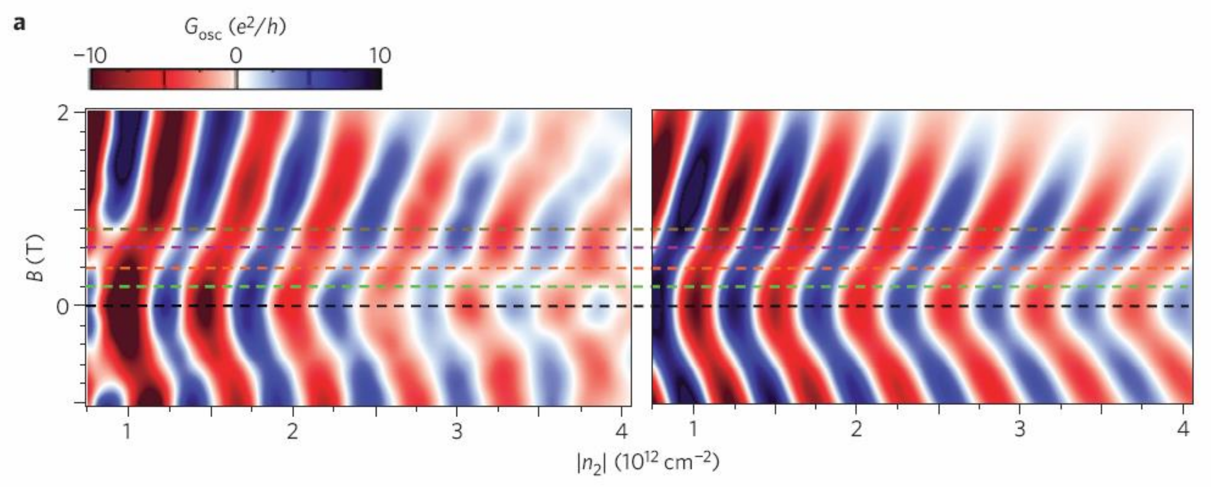

One-dimensional barrier

T. Tudorovskiy, K. Reijnders & MIK, 2012, 2013

One-dimensional potential

$$\left[v\begin{pmatrix} 0 & \hat{p}_x - ip_y \\ \hat{p}_x + ip_y & 0 \end{pmatrix} + u(x/l) - E\right]\Psi = 0$$

$$\tilde{x} = x/l,\ \tilde{p}_x = -ihd/d\tilde{x},\ \tilde{p}_y = p_y/p_0,\ h = \hbar/p_0 l,\ \tilde{u} = u/vp_0$$

$$\widetilde{E} = E/vp_0$$

Skipping tildes: the Hamiltonian

$$\hat{H} = \begin{pmatrix} 0 & \hat{p}_x - ip_y \\ \hat{p}_x + ip_y & 0 \end{pmatrix} + u(x)$$

One-dimensional barrier II

Reduction to exact Schrödinger equations for complex potential

$$\left(\hat{p}_x^2 + p_y^2 - v(x)^2 - ih\sigma_x v'(x)\right)\Psi = 0$$

$$v(x) = u(x) - E$$

$$\Psi = \begin{pmatrix} 1 \\ 1 \end{pmatrix} \eta_1 + \begin{pmatrix} 1 \\ -1 \end{pmatrix} \eta_2$$

$$\left(h^2 \frac{d^2}{dx^2} + v(x)^2 - p_y^2 \pm ihv'(x)\right) \eta_{1,2} = 0$$

Schròdinger equation with complex potential

Classical equations

Classical dynamics is described by the Hamiltonian

$L_0^{\pm}(p_x, x) = \pm|\mathbf{p}| + u(x)$ for electrons and holes

Turning points $u(x_0) = E$

Electron and hole Hamiltonians coincide for normal incidence:

$$p_x = p_y = 0$$

Squared Hamiltonian equations: $\mathcal{L}(p_x, x) \equiv p_x^2 - v^2(x) = -p_y^2$

$\epsilon = -p_y^2$ plays the role of energy

Semiclassical theory

Exact equations (continued to the complex plane $x \to z$)

$$\left(h^2 \frac{d^2}{dz^2} + v^2(z) - p_y^2 + ihv'(z) \right) \eta_1(z) = 0$$

$$\eta_2 = \frac{1}{p_y} \left(h \frac{d}{dz} + iv(z) \right) \eta_1(z)$$

Semiclassical solution

$$\eta_1(z) = A(z,h) e^{is(z)/h}$$ $$A(z,h) = A_0(z) + hA_1(z) + \ldots$$

Semiclassical theory II

Fundamental semiclassical solutions

$$\eta_1(x) = \frac{a_1}{\sqrt{p_x(x)}\sqrt{G(x)}} e^{iS(x_0,x)/h} + a_2 \frac{\sqrt{G(x)}}{\sqrt{p_x(x)}} e^{-iS(x_0,x)/h}$$

$$\eta_2(x) = i\alpha_v \frac{|p_y|}{p_y} \left(a_1 \frac{\sqrt{G(x)}}{\sqrt{p_x(x)}} e^{iS(x_0,x)/h} + a_2 \frac{1}{\sqrt{p_x(x)}\sqrt{G(x)}} e^{-iS(x_0,x)/h} \right)$$

$$G(x) = \left(\frac{|v(x)| + p_x(x)}{|p_y|} \right)^{\alpha_v}, \quad \alpha_v = \mathrm{sgn}[v(x_0)]$$

$$p_x(x) = \sqrt{v^2(x) - p_y^2}, \quad S(x_0, x) = \int_{x_0}^{x} p_x(\zeta) d\zeta$$

Stokes diagrams

The semiclassical solutions are divergent at the turning points

$$p_x(z_0) = 0$$

The matching of solutions in various regions can be done in complex plane when we can go around the turning point at some safe distance

General complex WKB: $$h^2 \frac{d^2\psi}{dz^2} + q(z)\psi(z) = 0 \qquad h \ll 1$$

Fundamental semiclassical solutions

$$f_1(z_0, z) = q^{-1/4} \exp\left(\frac{i}{h}\int_{z_0}^{z} dz'\, q^{1/2}(z')\right),$$

$$f_2(z_0, z) = q^{-1/4} \exp\left(-\frac{i}{h}\int_{z_0}^{z} dz'\, q^{1/2}(z')\right)$$

Stokes diagrams II

$$s(z_0, z) = \int_{z_0}^{z} q^{1/2}(z')dz'$$

Anti-Stokes lines: the function *s* is real. Both fundamental solutions are comparable in their amplitude at these lines.

(Stokes lines: the function *s* is imaginary – less important)

At each anti-Stokes lines $\psi(z) = C_1^{\gamma} f_1(z_0, z) + C_2^{\gamma} f_2(z_0, z)$

Stokes phenomenon: there are jumps in the coefficients (and they are roughly associated to Stokes lines)

So, the exact solution has different representations in different sectors of the complex plane

Stokes diagrams III

Scattering problem: connecting propagating (not evanescent!) waves in different regions, that is, transition from one anti-Stokes line to the other anti-Stokes line, that is, calculation of connection matrix

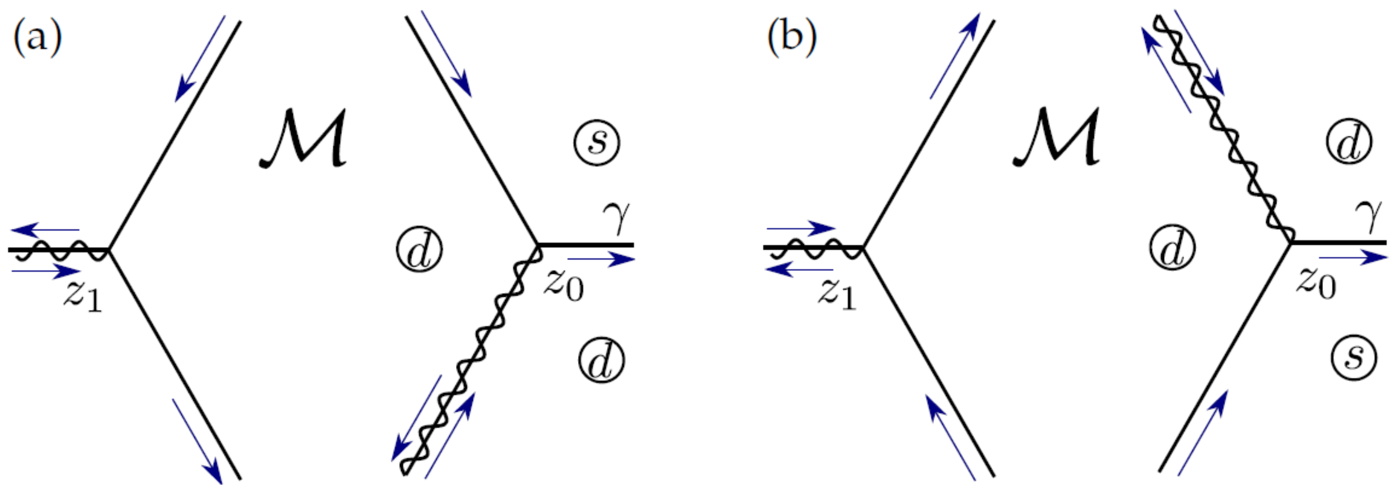

Figure 2.5: The Stokes diagram for two simple turning points z_0 and z_1. The blue arrows show the direction in which the action $s(z_0, z)$ increases and the wavy lines depict the branch cuts. The division of the different sectors in dominant or subdominant is performed with respect to z_0. In diagram (a), we consider $\eta_1(z) = \eta_1^+(z)$ along γ and in diagram (b) we consider $\eta_1(z) = \eta_1^-(z)$ along γ.

Different cases

1. $E < u_0$, $|p_y| < u_0 - E$: Klein tunneling regime, or tunneling through a barrier supporting hole states
2. $E > u_0$, $|p_y| < E - u_0$: above-barrier scattering
3. $E < u_0$ and $|p_y| > u_0 - E$, or $E > u_0$, $|p_y| > E - u_0$: conventional tunneling regime, tunneling through a barrier without hole states.

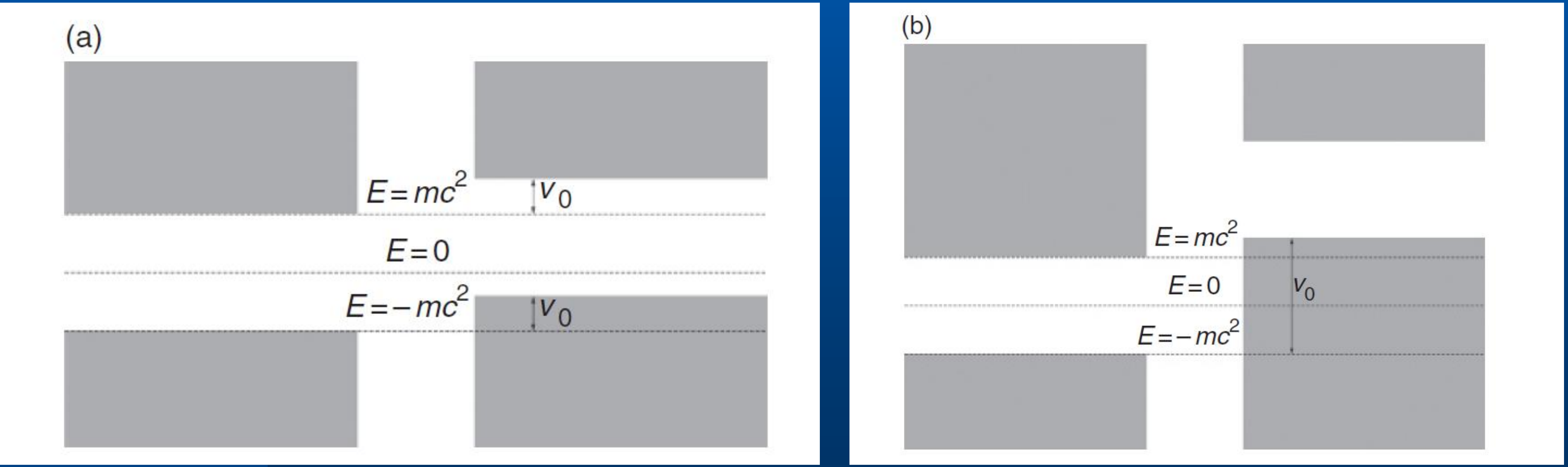

Difference between conventional case and Klein tunneling for real Dirac particles

Different cases II

Classical mechanics: $E = \pm|\boldsymbol{p}| + u(x)$

Effective Hamiltonian $\mathcal{L}(p_x, x) = p_x^2 - v^2(x) = -p_y^2$

$v(x) = u(x) - E$

The case of Klein tunneling $E < U_{\max}, \; |p_y| < U_{\max} - E$

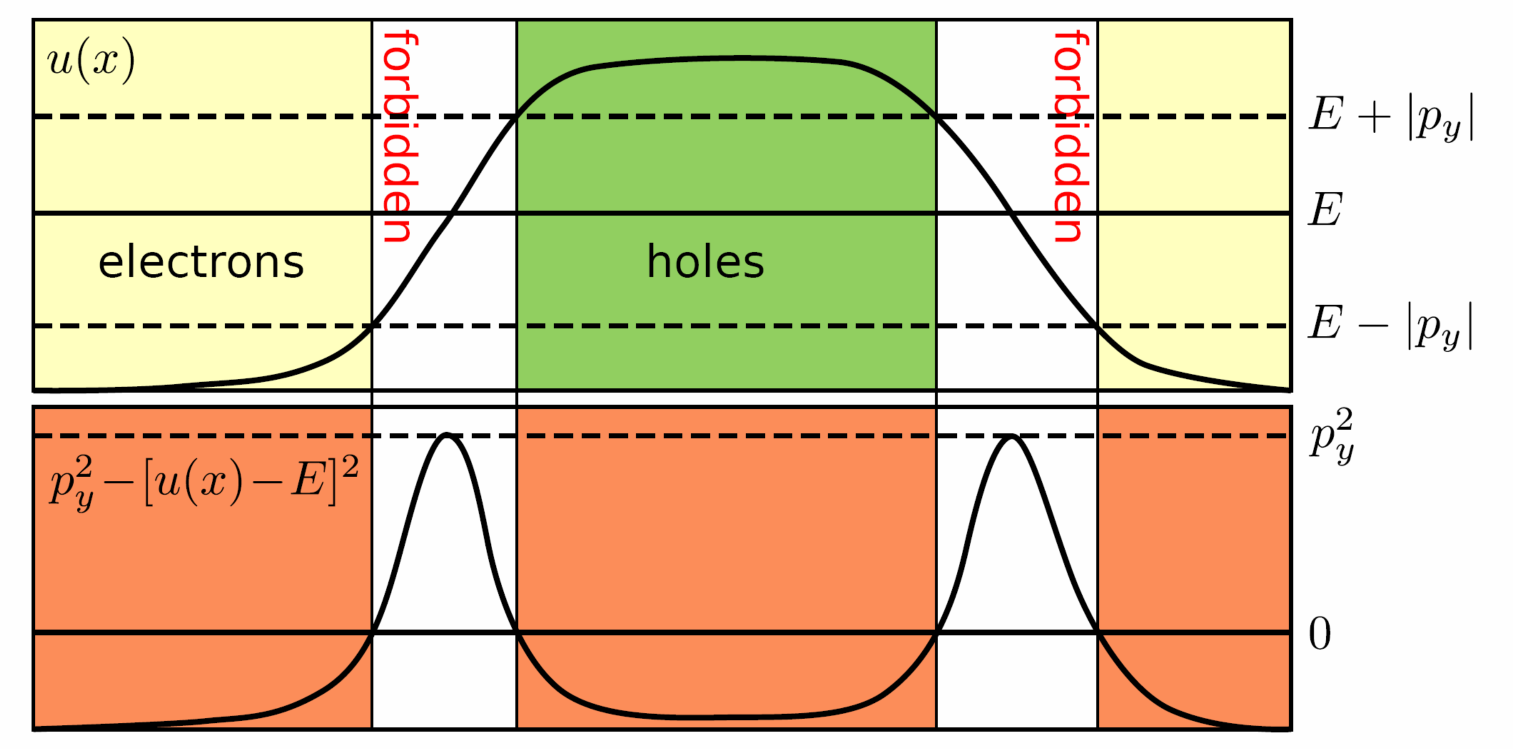

Different cases III

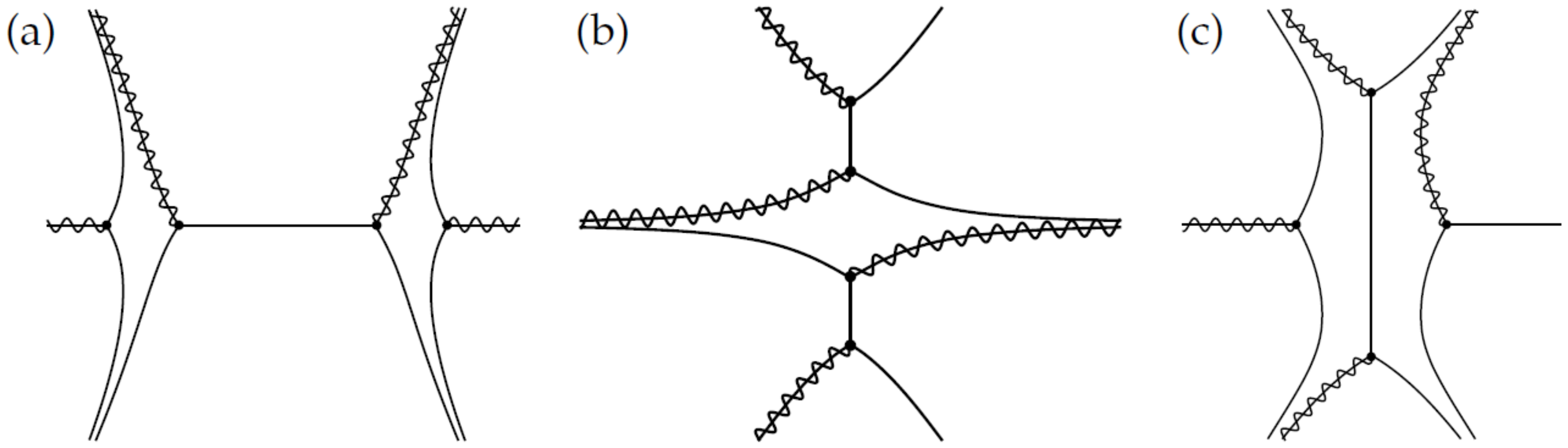

Figure 2.3: Stokes diagrams for the three different regimes outlined in section 2.2: (a) Klein tunneling, (b) above-barrier scattering and (c) conventional tunneling. Bold points show the turning points, the solid lines correspond to anti-Stokes lines and the wavy lines designate branch cuts of the function $(z - z_0)^{1/2}$. This figure was created using the potential $u(z) = -z^2$.

Klein tunneling – four real turning points; above-barrier scattering – four complex turning points

Method of comparison equations

$$h^2 \frac{d^2 \psi}{dz^2} + R(z,h)\psi(z) = 0$$

$$R(z,h) = \sum_{n=0}^{\infty} R_n(z) h^n$$

Map it to a related equation

$$h^2 \frac{d^2 V}{d\phi^2} + Q(\phi,h) V(\phi) = 0$$

which we can hope to solve (Q will be specified later)

$$\psi(z,h) = (\phi'(z))^{-1/2} V(\phi(z))$$

$\phi(z)$ is non-singular, i.e. ϕ' does not vanish

$$h^2 \left(\frac{3}{4} \frac{(\phi'')^2}{(\phi')^2} - \frac{\phi'''}{2\phi'} \right) - Q(\phi,h)(\phi')^2 + R(z,h) = 0$$

Method of comparison equations II

$$Q(\phi,h)=\sum_{n=0}^{\infty}Q_n(\phi)h^n$$

$$\phi(z,h)=\sum_{n=0}^{\infty}\phi_n(z)h^n.$$

and compare term by term:

$$Q_0(\phi_0)(\phi_0')^2=R_0(z)$$

$Q_0(\phi_0)$ and $R_0(z)$ have the same number of turning points

$$Q_1(\phi_0)(\phi_0')^2+Q_0'(\phi_0)\phi_1(\phi_0')^2+2Q_0(\phi_0)\phi_0'\phi_1'=R_1(z)$$

$$\phi_1(z)=\frac{1}{2}\phi_0'R_0^{-1/2}\int_{z_0}^{z}dz'\,R_0^{-1/2}\left(R_1-(\phi_0')^2Q_1(\phi_0)\right)$$

etc., term by term

Method of comparison equations III

Suppose R_0 has zeros (turning points) of the order m_j at $z = z_j$

Then, Q can be choosen as a polynomial:

$$Q_0(\phi) = \gamma_{\mu 0} \prod_{j=0}^{N} (\phi - \phi_0(z_j))^{m_j}$$

$$\int_{\phi_0(z_0)}^{\phi_0(z)} ds \prod_{j=0}^{N} [s - \phi_0(z_j)]^{m_j/2} = \int_{z_0}^{z} dz' \, [\gamma_{\mu 0}^{-1} R_0(z')]^{1/2}$$

Putting $z = z_j$ we find all constants $\phi_0(z_j)$ except one

We will consider *quadratic* polynom (Eqs. for Weber functions)

Application to Dirac equation

The expression for scattering matrix for n-p and p-n junctions:

$$T_{np} = \begin{pmatrix} e^{K/h} & \sqrt{e^{2K/h} - 1}\, e^{-i\theta - i\pi/2} \\ \sqrt{e^{2K/h} - 1}\, e^{i\theta - i\pi/2} & -e^{K/h} \end{pmatrix}$$

$$T_{pn} = \begin{pmatrix} e^{K/h} & \sqrt{e^{2K/h} - 1}\, e^{i\theta + i\pi/2} \\ \sqrt{e^{2K/h} - 1}\, e^{-i\theta + i\pi/2} & -e^{K/h} \end{pmatrix}$$

$$K = \int_{x_-}^{x_+} \sqrt{p_y^2 - v^2(x)}dx$$

$$\theta = \mathrm{Arg}\left[\Gamma\left(1 + i\frac{K}{\pi h}\right)\right] - \frac{\pi}{4} + \frac{K}{\pi h} - \frac{K}{\pi h}\ln\left(\frac{K}{\pi h}\right)$$

p-n-p junction

Comparison equation with four turning points is too complicated, and no analytical solution is known, therefore we consider p-n and n-p junctions separately

Transmission probability

$$t_{npn} = \frac{e^{-K_{np}/h} e^{-K_{pn}/h} e^{-iL/h}}{1 - \sqrt{1 - e^{-K_{np}/h}} \sqrt{1 - e^{-K_{pn}/h}} e^{-2iL/h + i\pi - i\theta_{np} - i\theta_{pn}}}$$

$$K_{np} = \int_{x_1}^{x_2} dx \sqrt{p_y^2 - v^2(x)}$$

$x_{1,2}$ are turning points

$$v^2(x_0) - p_y^2 = 0$$

$$L = \int_{x_2}^{x_3} dx' \sqrt{v^2(x') - p_y^2}$$

$$\theta = \mathrm{Arg}\left[\Gamma\left(1 + i\frac{K}{\pi h}\right)\right] - \frac{\pi}{4} + \frac{K}{\pi h} - \frac{K}{\pi h} \ln\left(\frac{K}{\pi h}\right)$$

Fabri-Perot resonances

Magic angles with 100% transmission survives only for symmetric barriers (except normal incidence)

$$|t_{\mathrm{res}}| = \frac{1}{\cosh(K_{np}/h - K_{pn}/h)}$$

$$K_{np}/h \gg 1,\ K_{pn} \gg 1$$

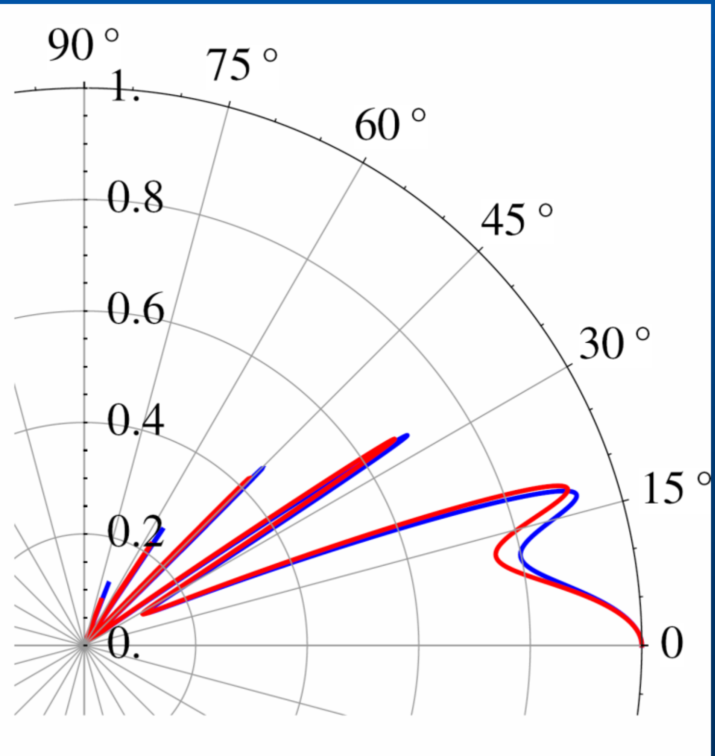

$$u(x/l_1) = \frac{U_{max}}{2}\left[1 + \tanh\left(10\frac{x}{l_1} - 5\right)\right]$$

The angular dependence of the transmission coefficient for a particle of energy 80 meV incident on an n-p-n junction of height 200 meV. The barrier width $l_2 = 250$ nm and the n-p and p-n regions have characteristic lengths $l_1 = 150$ nm and $l_3 = 50$ nm, respectively. The blue line shows the numerical results for 99 steps, while the red line shows the uniform approximation (5.77).

Very nice agreement with numerics

Klein tunneling and Veselago lensing

If refraction index is negative the flat interface works like lens (V.S. Veselago, 1968)

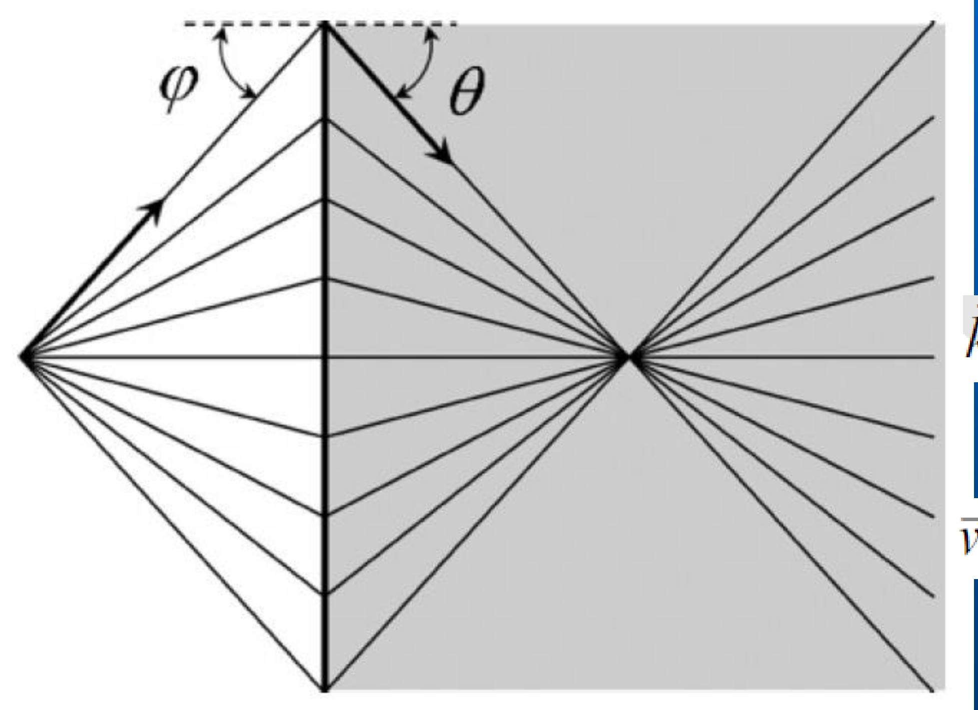

Group velocity $\vec{v}_g = \pm v \frac{\vec{k}}{k}$

In electron region:

$\vec{k} = k(\cos\varphi, \sin\varphi)$ $\vec{v}_e = v(\cos\varphi, \sin\varphi)$

In hole region:

$\vec{v}_h = v(\cos\theta', \sin\theta')$ $\vec{q} = -q(\cos\theta', \sin\theta')$

$\theta' = -\theta$

$$\frac{\sin\theta'}{\sin\varphi} = -\frac{k}{q} \equiv n$$

is negative

Graphene with p-n junction as electronic metamaterial

Cheianov, Fal'ko, Altshuler, Science 315, 1252 (2007)

Veselago lens for massless Dirac fermions

Reijnders & MIK, Phys. Rev. B 95, 115310 (2017)

Green function $$[v_F \boldsymbol{\sigma} \cdot \hat{\mathbf{p}} + U(\mathbf{x})1_2]G(\mathbf{x},\mathbf{x}_0) = EG(\mathbf{x},\mathbf{x}_0) + \delta(\mathbf{x}-\mathbf{x}_0)1_2$$

Wave function from initially polarized source $$\Psi(\mathbf{x}) = G(\mathbf{x},\mathbf{x}_s)\begin{pmatrix}\alpha_1 \\ \alpha_2\end{pmatrix}$$

U is just a potential step $$U(\mathbf{x}) = U(x) = U_0\Theta(x)$$ Source: $\mathbf{x}_s = (x_s, 0)$

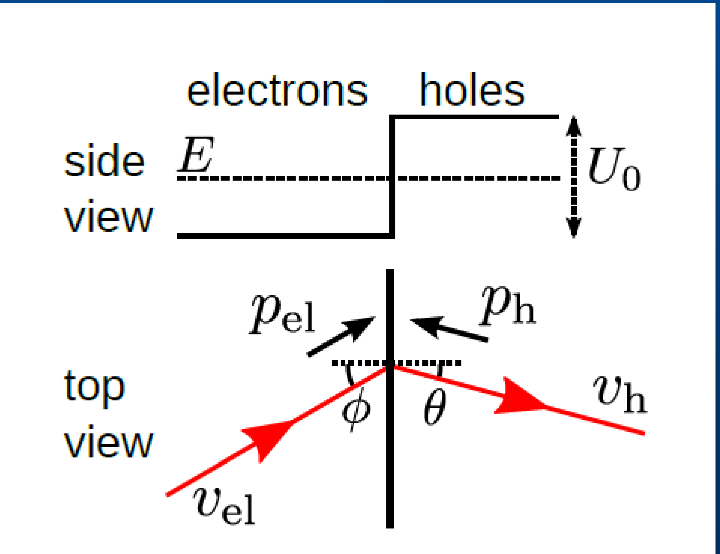

$$\frac{\sin\phi}{\sin\theta} = -\frac{p_h}{p_e} = -\frac{U_0 - E}{E} \equiv n$$

Veselago lens for Dirac fermions II

Classical Hamiltonian $H_{cl}^{\pm} = \pm|\mathbf{p}| + U(\mathbf{x})$

Classical action $S_{np}(p_y, x, y) = -x_s\sqrt{E^2 - p_y^2} - x\sqrt{(E-U_0)^2 - p_y^2} + yp_y$

Classical trajectories

$$y = -x_s \frac{p_y}{\sqrt{E^2 - p_y^2}} - x \frac{p_y}{\sqrt{(E-U_0)^2 - p_y^2}}$$

$$= -x_s \tan\phi + x \tan\theta.$$

Singular points (caustics): $\partial^2 S_{np}/\partial p_y^2$ vanishes

They form the lines (caustics) where density of trajectories is divergent

Veselago lens for Dirac fermions III

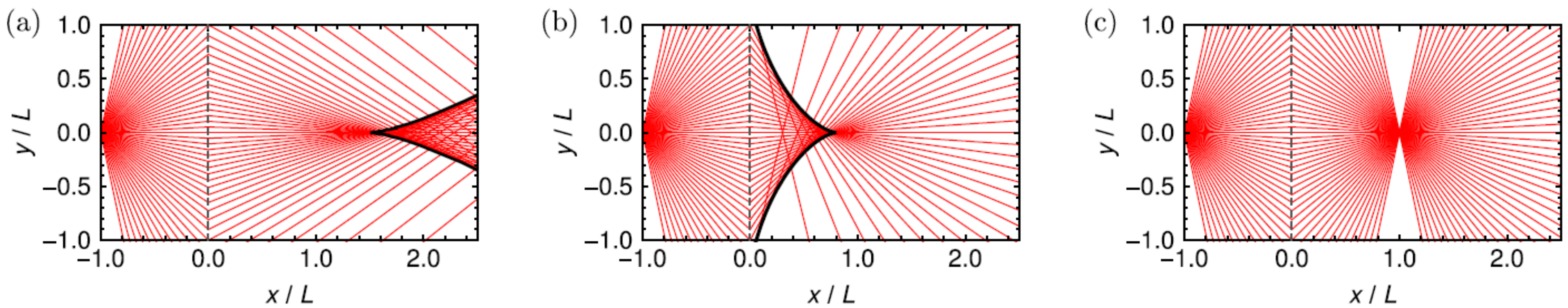

FIG. 1. The classical trajectories (red lines) for massless Dirac fermions that are emitted by a point source and are incident on an *n*-*p* junction at $x = 0$ (dashed gray line). We see that the junction focusses the particles. The solid black line indicates the caustic, which is the envelope of the classical trajectories, and separates the region where each point lies on a single trajectory from the region where each point lies on three trajectories. It consists of twofold lines meeting into a cusp point at $(x_{\mathrm{cusp}},0)$. (a) For $U_0 > 2E$, the cusp point $x_{\mathrm{cusp}} > -x_s$ is the left-most point of the caustic. (b) When $U_0 < 2E$, the cusp point $x_{\mathrm{cusp}} < -x_s$ is the right-most point of the caustic. (c) For $U_0 = 2E$, all trajectories are focused into a single point.

$U_0 = 2E$ is an exceptional case, $n = -1$, ideal focus
(the caustics shrink to a single point)

Interference patterns

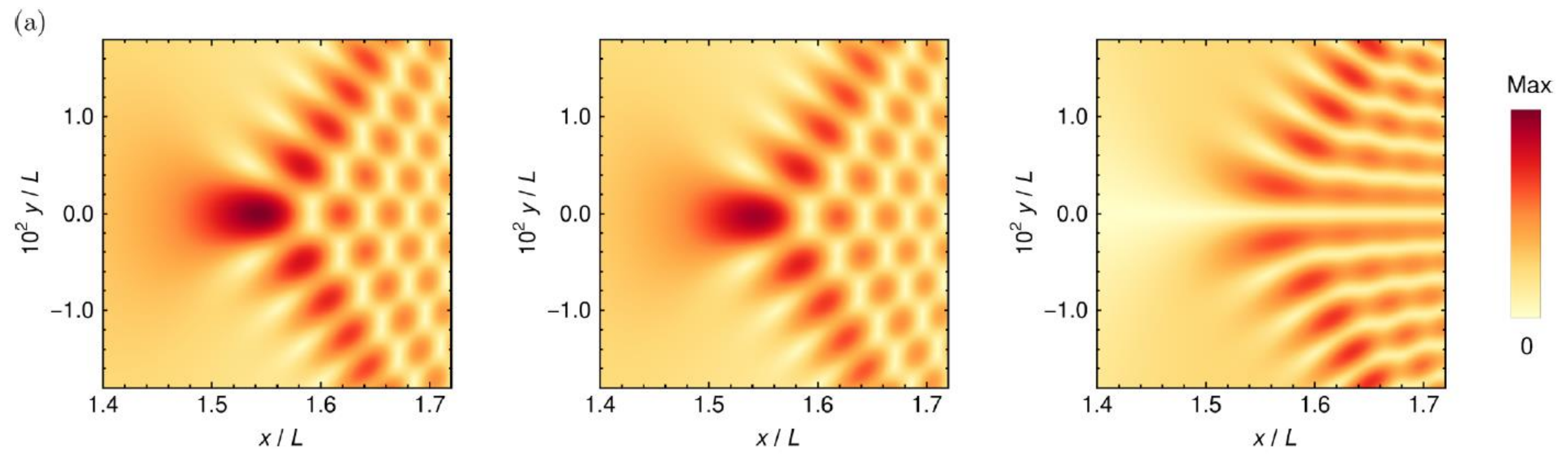

FIG. 7. The density $\|\Psi\|$ for the dimensionless parameters $U_0 = 2.5$ and $h = 0.000639$. For graphene, these numbers correspond to $E = 100$ meV, $U_0 = 250$ meV, and $L = 10^4$ nm. (a) The exact result obtained by numerically evaluating the exact wave function (16). (b)

The left, middle, and right panels correspond to three different polarizations (α_1, α_2), to wit $(1,1)/\sqrt{2}$; $(1,0)$ and $(1,-1)/\sqrt{2}$.

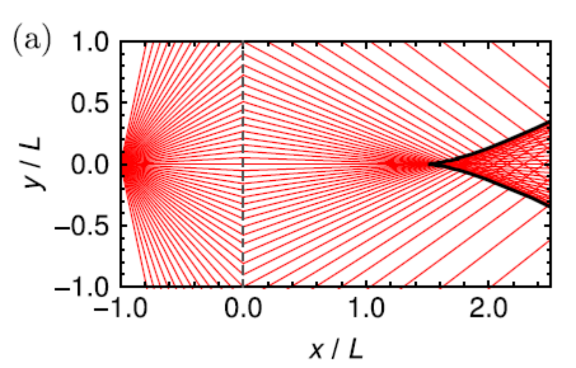

$U_0 > 2E$

Pseudospin polarization and symmetry breaking

$$S_{np}(x,-y,-p_y) = S_{np}(x,y,p_y)$$

$$G(x,-y,x_0,-y_0) = \sigma_x G(x,y,x_0,y_0)\sigma_x$$

$$\begin{aligned} \|\Psi(x,-y)\|^2 &= \left\|\sigma_x G(x,y,x_s,0)\sigma_x \begin{pmatrix} \alpha_1 \\ \alpha_2 \end{pmatrix}\right\|^2 \\ &= \left\|G(x,y,x_s,0) \begin{pmatrix} \alpha_2 \\ \alpha_1 \end{pmatrix}\right\|^2 . \end{aligned}$$

This is equal to $\|\Psi(x,y)\|^2$ only if $\alpha_1 = \pm\alpha_2$

(Pseudo)spin polarization breaks the mirror symmetry!

Pseudospin polarization and symmetry breaking II

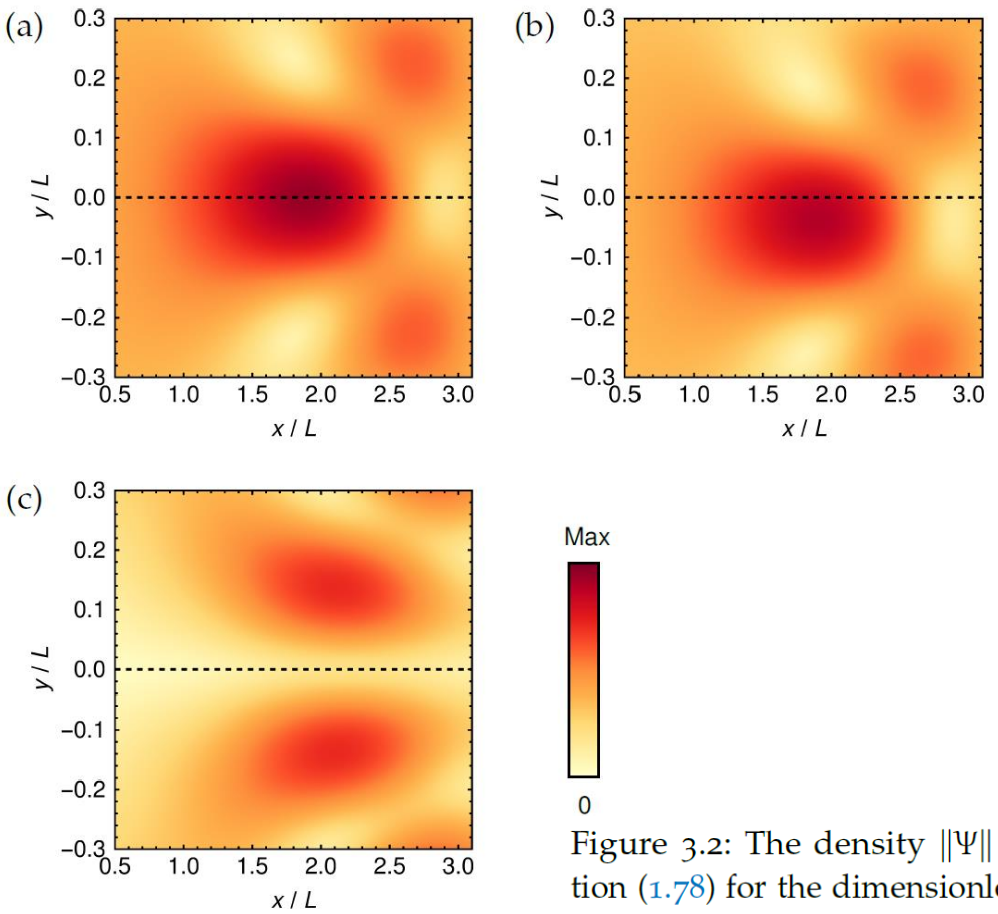

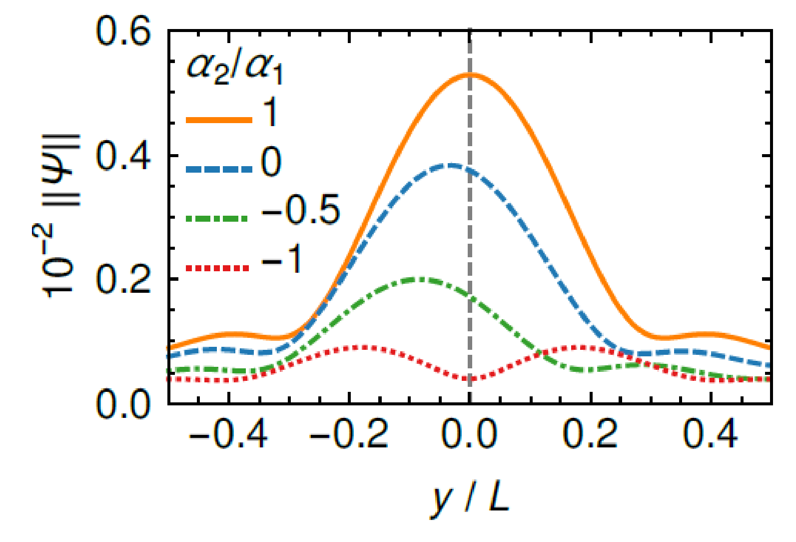

$x = x_{cusp}$

Figure 3.2: The density $\|\Psi\|$ computed by numerically evaluating the exact wavefunction (1.78) for the dimensionless parameters $U_0 = 2.5$ and $h = 0.0639$. For graphene, these numbers correspond to $E = 100$ meV, $U_0 = 250$ meV and $L = 100$ nm. We consider three different polarizations. (a) For $(\alpha_1, \alpha_2) = (1, 1)/\sqrt{2}$, the density is symmetric about the x-axis. (b) When $(\alpha_1, \alpha_2) = (1, 0)$, this symmetry is no longer there and the maximum lies at $y < 0$. (c) For $(\alpha_1, \alpha_2) = (1, -1)/\sqrt{2}$, the density is symmetric again, but the central resonance has disappeared. The maximum of the color scale equals (a) 70, (b) 55 and (c) 22.

WKB approximation

$$\Psi(x,y) = \iint G(x,y,x_0,y_0) J(x_0,y_0) \mathrm{d}x_0 \mathrm{d}y_0$$

$$J(x,y) = \begin{pmatrix} \alpha_1 \\ \alpha_2 \end{pmatrix} \delta(x+L)\delta(y)$$

Green's function

$$G(x,y,x_0,y_0) \propto \int \underbrace{\frac{\mathrm{d}p_y}{\cos\frac{\phi+\theta}{2}} \begin{pmatrix} e^{i(\phi-\theta)/2} & e^{-i(\phi+\theta)/2} \\ e^{i(\phi+\theta)/2} & e^{-i(\phi-\theta)/2} \end{pmatrix}}_{\text{Amplitude } f(p_y)} \underbrace{e^{iS_{np}(x,y,x_0,y_0)/h}}_{\text{Action } S_{\text{np}}}$$

$$S_{\text{np}}(x,y,x_0,y_0) = |x_0|\sqrt{E^2 - p_y^2} - x\sqrt{(U_0-E)^2 - p_y^2} + (y-y_0)p_y$$

h is small: we need to calculate fastly oscillating integrals

WKB approximation II

$$I(\mathbf{x}, h) = \int_{-\infty}^{\infty} d\eta\, f(\mathbf{x}, \eta) e^{iS(\mathbf{x},\eta)/h}$$

$$h \to 0$$

Main contribution is from stationary points $\left.\frac{\partial S}{\partial \eta_i}\right|_{(\mathbf{x}_0,\boldsymbol{\eta}_0)} = 0, \quad i = 1 \ldots n$

Generic case:

$$\det A(\mathbf{x}_0, \boldsymbol{\eta}_0) \equiv \det \left.\frac{\partial^2 S}{\partial \eta_i \partial \eta_j}\right|_{(\mathbf{x}_0,\boldsymbol{\eta}_0)} \neq 0$$

$$I(\mathbf{x}, h) = (2\pi h)^{n/2} \frac{f(\mathbf{x}_0, \boldsymbol{\eta}_0)}{\sqrt{|\det A(\mathbf{x}_0, \boldsymbol{\eta}_0)|}} e^{i\pi\,\mathrm{sgn}(A(\mathbf{x}_0,\boldsymbol{\eta}_0))/4} \times e^{iS(\mathbf{x}_0,\boldsymbol{\eta}_0)/h}(1 + \mathcal{O}(h))$$

In QM it corresponds to WKB approximation

Does not work near caustics or cusps!

Airy approximation I

Fold caustics: Airy approximation $\left.\frac{\partial S}{\partial \eta}\right|_{(\mathbf{x}_0,\eta_0)} = 0, \quad \text{and} \quad \left.\frac{\partial^2 S}{\partial \eta^2}\right|_{(\mathbf{x}_0,\eta_0)} = 0$

Expand to the higher (third) order:

$$\begin{aligned} S(\mathbf{x},\eta) &= S^{(3)}(\mathbf{x},\eta) + \mathcal{O}(\beta^4) \\ &= q_0(\mathbf{z}) + q_1(\mathbf{z})\beta + \frac{q_2(\mathbf{z})}{2}\beta^2 + \frac{q_3(\mathbf{z})}{6}\beta^3 + \mathcal{O}(\beta^4) \end{aligned}$$

$$\beta = \eta - \eta_0$$

$$\mathbf{z} = \mathbf{x} - \mathbf{x}_0$$

$$\begin{aligned} &q_0(\mathbf{z}) = a_0 + \langle \mathbf{b}_0, \mathbf{z}\rangle + \mathcal{O}(z^2), && q_1(\mathbf{z}) = \langle \mathbf{b}_1, \mathbf{z}\rangle + \mathcal{O}(z^2), \\ &q_2(\mathbf{z}) = \langle \mathbf{b}_2, \mathbf{z}\rangle + \mathcal{O}(z^2), && q_3(\mathbf{z}) = a_3 + \mathcal{O}(z). \end{aligned}$$

Airy approximation II

$$I(\mathbf{x},h) = \int_{-\infty}^{\infty} d\eta\, f(\mathbf{x},\eta_0) e^{iS^{(3)}(\mathbf{x},\eta)/h} + \mathcal{O}(h^{2/3}),$$

$$= 2\pi f(\mathbf{x},\eta_0) \sqrt[3]{\frac{2h}{|q_3|}} \exp\left[\frac{i}{h}\left(q_0 + \frac{q_2^3}{3q_3^2} - \frac{q_1 q_2}{q_3}\right)\right]$$

$$\times \mathrm{Ai}\left[\frac{2^{1/3}}{h^{2/3} q_3^{1/3}}\left(q_1 - \frac{q_2^2}{2q_3}\right)\right] + \mathcal{O}(h^{2/3})$$

is expressed via Airy function

$$\mathrm{Ai}(u) = \frac{1}{2\pi}\int_{-\infty}^{\infty} \exp\left(\frac{i}{3}t^3 + iut\right) dt$$

Airy approximation III

$$q_0 + \frac{q_2^3}{3q_3^2} - \frac{q_1 q_2}{q_3} = a_0 + \langle \mathbf{b}_0, \mathbf{z} \rangle + \mathcal{O}(z^2),$$

$$\frac{2^{1/3}}{h^{2/3} q_3^{1/3}} \left(q_1 - \frac{q_2^2}{2q_3} \right) = \frac{2^{1/3} \langle \mathbf{b}_1, \mathbf{z} \rangle}{h^{2/3} a_3^{1/3}} + \frac{\mathcal{O}(z^2)}{h^{2/3}}$$

The answer:

$$I(\mathbf{x}, h) = 2\pi f(\mathbf{x}_0, \eta_0) \sqrt[3]{\frac{2h}{|a_3|}} \exp\left[\frac{i}{h} (a_0 + \langle \mathbf{b}_0, \mathbf{z} \rangle) \right] \times \mathrm{Ai} \left(\frac{2 \langle \mathbf{b}_1, \mathbf{z} \rangle}{2^{2/3} h^{2/3} a_3^{1/3}} \right) + \mathcal{O}(h^{2/3})$$

Does not work near cusp!

Pearcey approximation

Near cusp, third derivative disappears as well

$$S(\mathbf{x},\eta) = S^{(4)}(\mathbf{x},\eta) + \mathcal{O}(\beta^5) = q_0(\mathbf{z}) + q_1(\mathbf{z})\beta + \frac{q_2(\mathbf{z})}{2}\beta^2 + \frac{q_3(\mathbf{z})}{6}\beta^3 + \frac{q_4(\mathbf{z})}{24}\beta^4 + \mathcal{O}(\beta^5)$$

$$I(\mathbf{x},h) = f(\mathbf{x}_0,\eta_0)\sqrt[4]{\frac{24h}{|a_4|}}\exp\left[\frac{i}{h}\left(a_0 + \langle \mathbf{b}_0,\mathbf{z}\rangle\right)\right] \times P^{\pm}\left[\sqrt{\frac{6}{h|a_4|}}\langle \mathbf{b}_2,\mathbf{z}\rangle, \sqrt[4]{\frac{24}{h^3|a_4|}}\langle \mathbf{b}_1,\mathbf{z}\rangle\right] + \mathcal{O}(h^{1/2})$$

Pearcey function

$$P^{\pm}(u,v) = \int_{-\infty}^{\infty} \exp\left(\pm i t^4 + i u t^2 + i v t\right)\, dt$$

Pearcey approximation II

Expand action up to 4^{th} order around $p_y = 0$ (not at ideal focus)

$$\Psi(x,y) \propto h^{1/4} f(0)\, \mathrm{P}^{\pm}\left[\sqrt{\frac{6}{h|a_4|}}\frac{x - x_{\text{cusp}}}{U_0 - E}, \sqrt[4]{\frac{24}{h^3|a_4|}}y\right]\left(1+\mathcal{O}\left(h^{1/4}\right)\right)$$

$$P^{\pm}(u,v) = \int d\eta \exp(\pm i\eta^4 + iu\eta^2 + iv\eta), \qquad a_4 = \left.\frac{\partial^4 S_{\text{np}}}{\partial p_y^4}\right|_{\substack{p_y=0,\\ \mathbf{x}=\mathbf{x}_{\text{cusp}}}}$$

Works only at small *h* but position of the main maximum is good

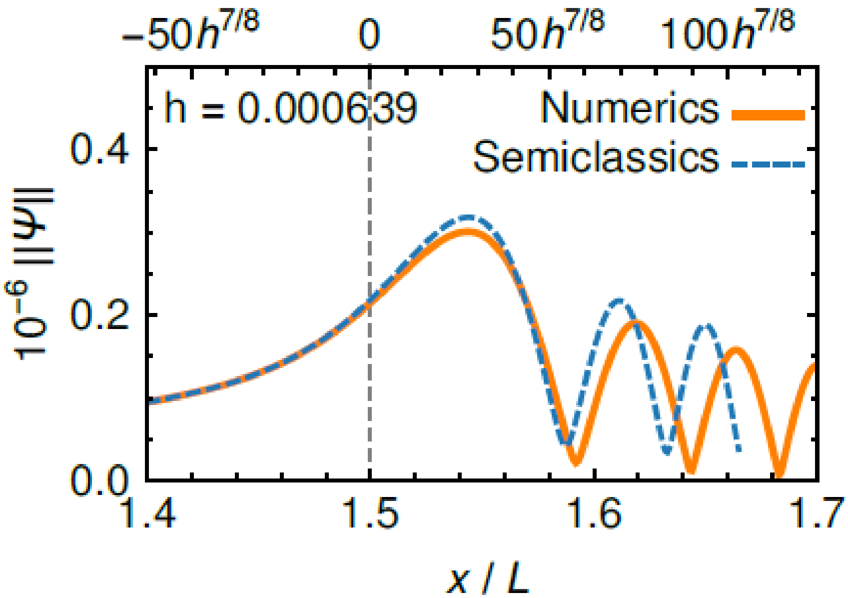

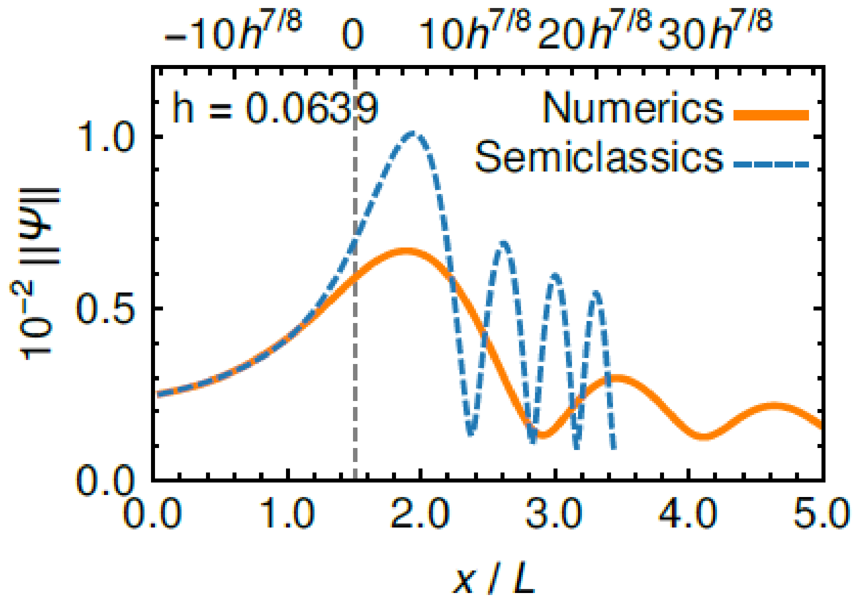

Semiclassical approximation

Exact

Pearcey (in ellipse); Airy (between dashed lines); WKB (outside)

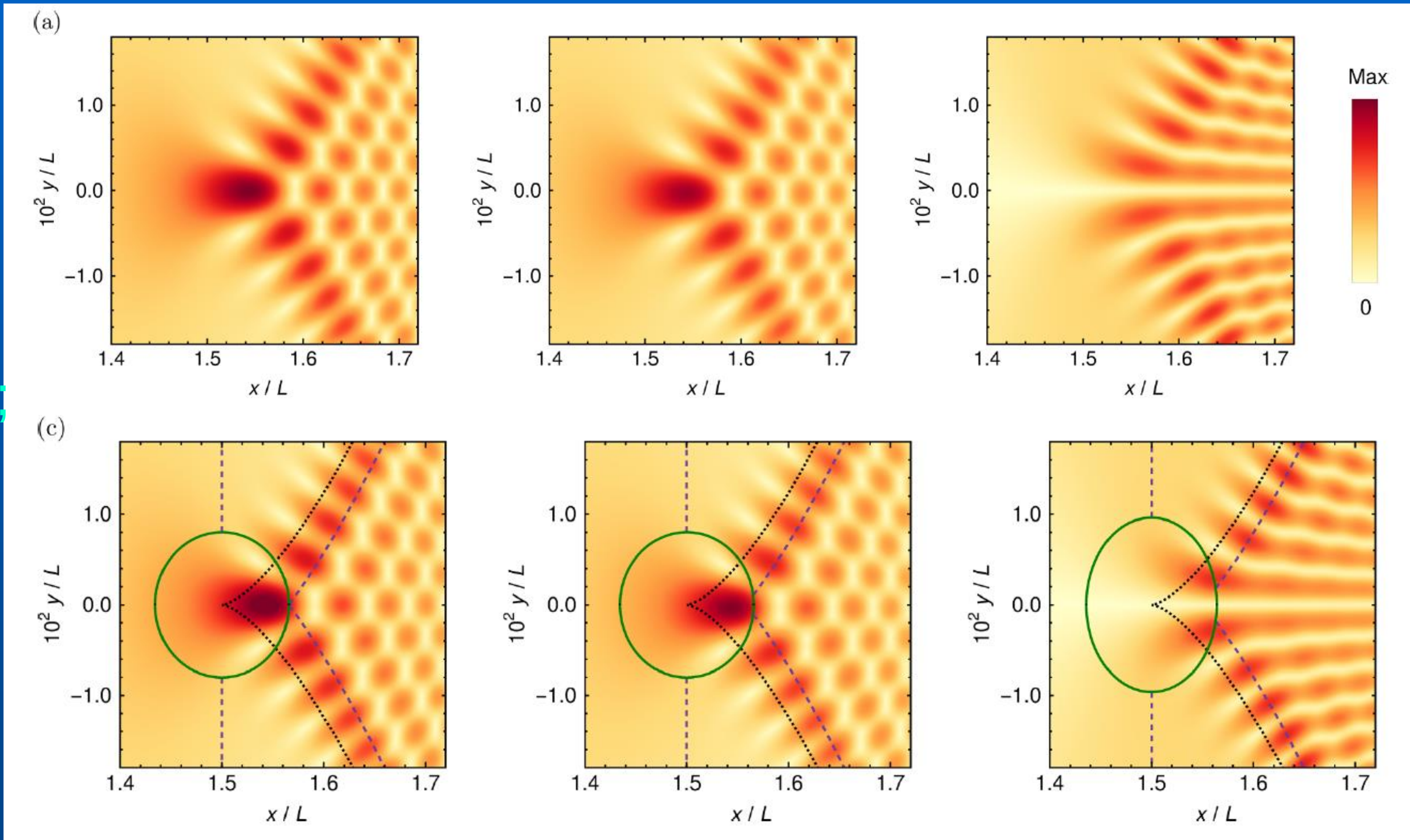

The density $\|\Psi\|$ for the dimensionless parameters $U_0 = 2.5$ and $h = 0.000639$

three different polarizations (α_1, α_2), to wit $(1,1)/\sqrt{2}$; $(1,0)$ and $(1,-1)/\sqrt{2}$.

Asymmetry in y direction

Pearcey function symmetric: include corrections

$$\Psi(x) = \int f(p_y) e^{iS_{np}(x,y,p_y)/h} \approx \int \left(f(0) + f'(0)p_y\right) e^{iS_{np}^{(4)}(x,y,p_y)/h} \mathrm{d}p_y$$

$$\propto h^{1/4}\left(f(0)\,P^{\pm}(\alpha,\beta) + h^{1/4}\,f'(0)\,P^{\pm}_{\beta}(\alpha,\beta) + \mathcal{O}\left(h^{1/2}\right)\right)$$

Expand $P^{\pm}$ to 2$^{\text{nd}}$ order in β, consider the cusp point ($\alpha = 0$)

Maximum of $\|\Psi\|^2$ at $y_{\max} = -\dfrac{h}{2E}\dfrac{\alpha_1 - \alpha_2}{\alpha_1 + \alpha_2} \overset{\text{restore}}{\underset{\text{units}}{=\!=\!=}} -\dfrac{\hbar v_F}{2E}\dfrac{\alpha_1 - \alpha_2}{\alpha_1 + \alpha_2}$

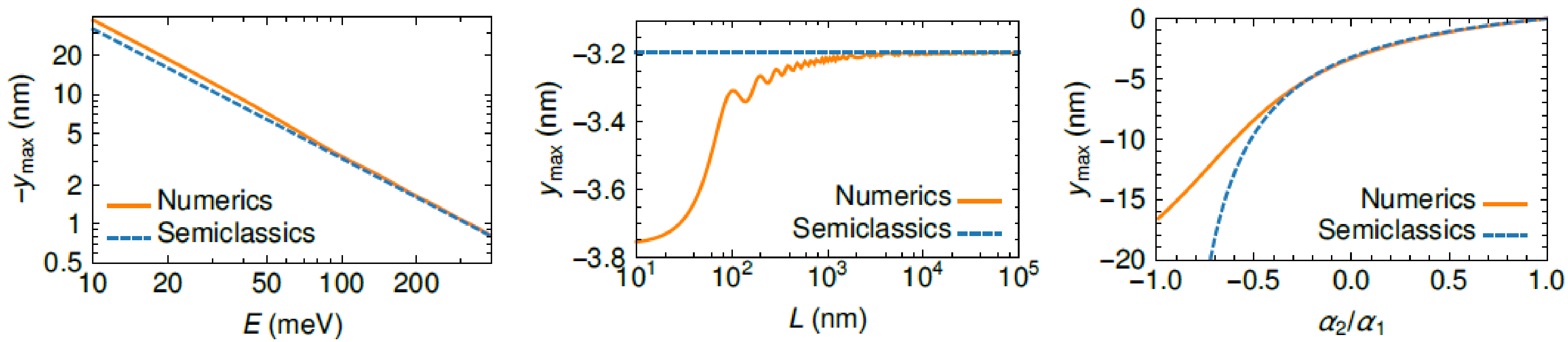

The effects of trigonal warping

Reijnders & MIK, Phys. Rev. B 96, 045305 (2017)

For Dirac fermions and $U_0 = 2E$ ideal focus

It is unstable in view of catastrophe theory

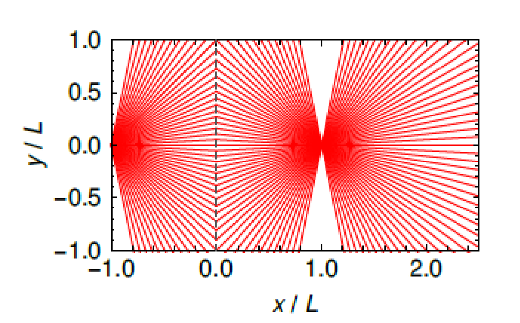

Trigonal warping: correction to the linear spectrum of graphene

$$E_\alpha^\pm = \pm\Big(|\mathbf{p}| + \alpha\mu|\mathbf{p}|^2 \cos\left[3(\phi_\mathbf{p} + \theta)\right]\Big), \qquad \mu \ll 1,\ \alpha = \pm 1$$

α is opposite for different valleys, *θ* depends on crystallographic orientation (*θ* = 0 corresponds to zigzag edges along x –direction)

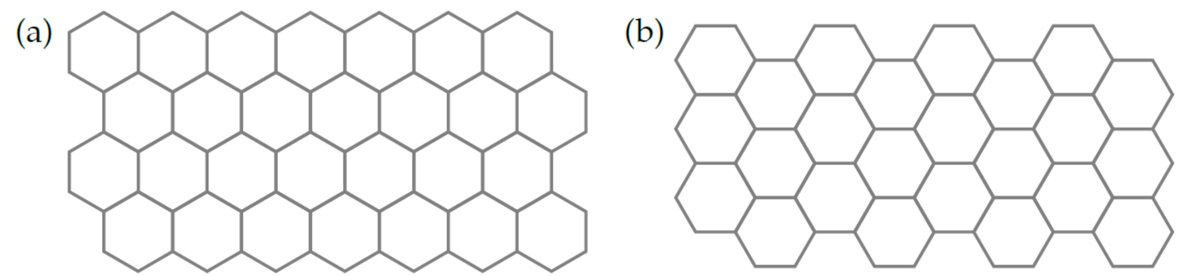

Figure 1.4: (a) Zigzag edges along the x-axis ($\theta = 0$). (b) Armchair edges along the x-axis ($\theta = \pi/6$).

The effects of trigonal warping II

Veselago lens with trigonal warping produces valley polarization*; in particular, the maxima of wave function are shifted

*Garcia-Pomar, Cortijo, Nieto-Vesperinas, Phys Rev Lett 100, 236801 (2008)

Semiclassical analysis similar to Dirac case + numerical TB simulations

K. J. A. REIJNDERS AND M. I. KATSNELSON PHYSICAL REVIEW B **96**, 045305 (2017)

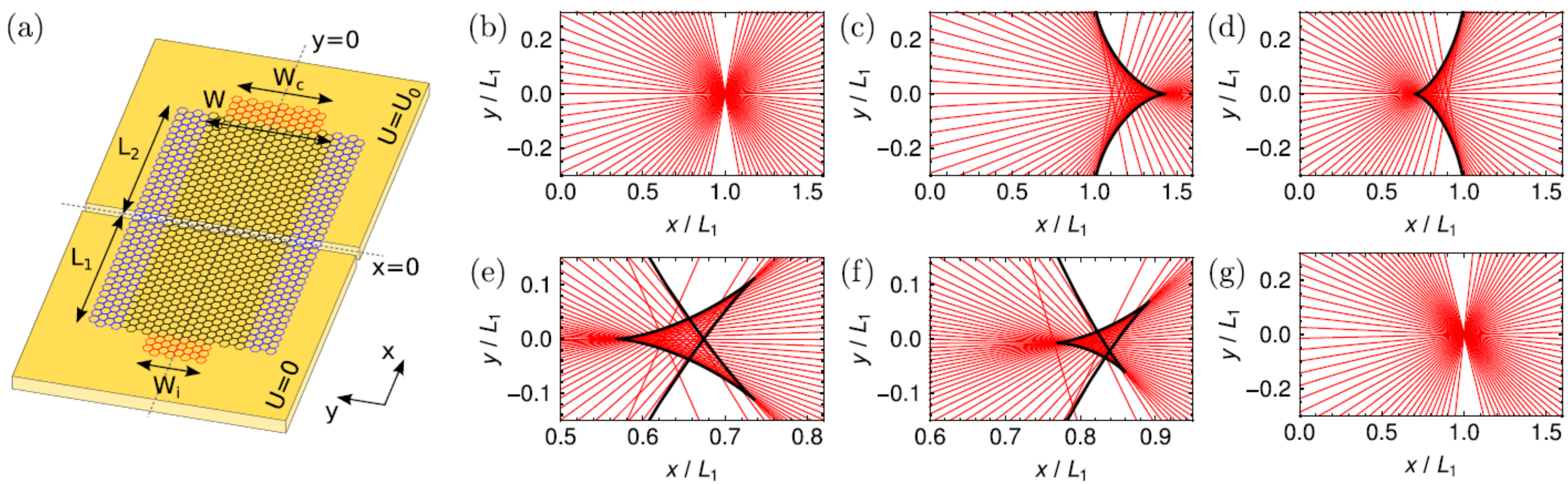

FIG. 1. (a) Simulation setup with an injector and collector lead (red) and drain leads on each side (blue). (b) Classical trajectories for the massless Dirac Hamiltonian at $U_0 = 2E$. (c)–(g) Classical trajectories (red) and caustics (black) for the Hamiltonian including trigonal warping. Unless otherwise indicated, $E = 0.4$ eV. (c) K valley, $U_0 = 0.8$ eV, $\theta = 0$; (d) K' valley, $U_0 = 0.8$ eV, $\theta = 0$; (e) section of the butterfly caustic. K' valley, $E = 0.6$ eV, $U_0 = 1.18$ eV, $\theta = 0$; (f) K' valley, $U_0 = 0.795$ eV, $\theta = \pi/12$; (g) $U_0 = 0.8$ eV, $\theta = \pi/6$.

The effects of trigonal warping III

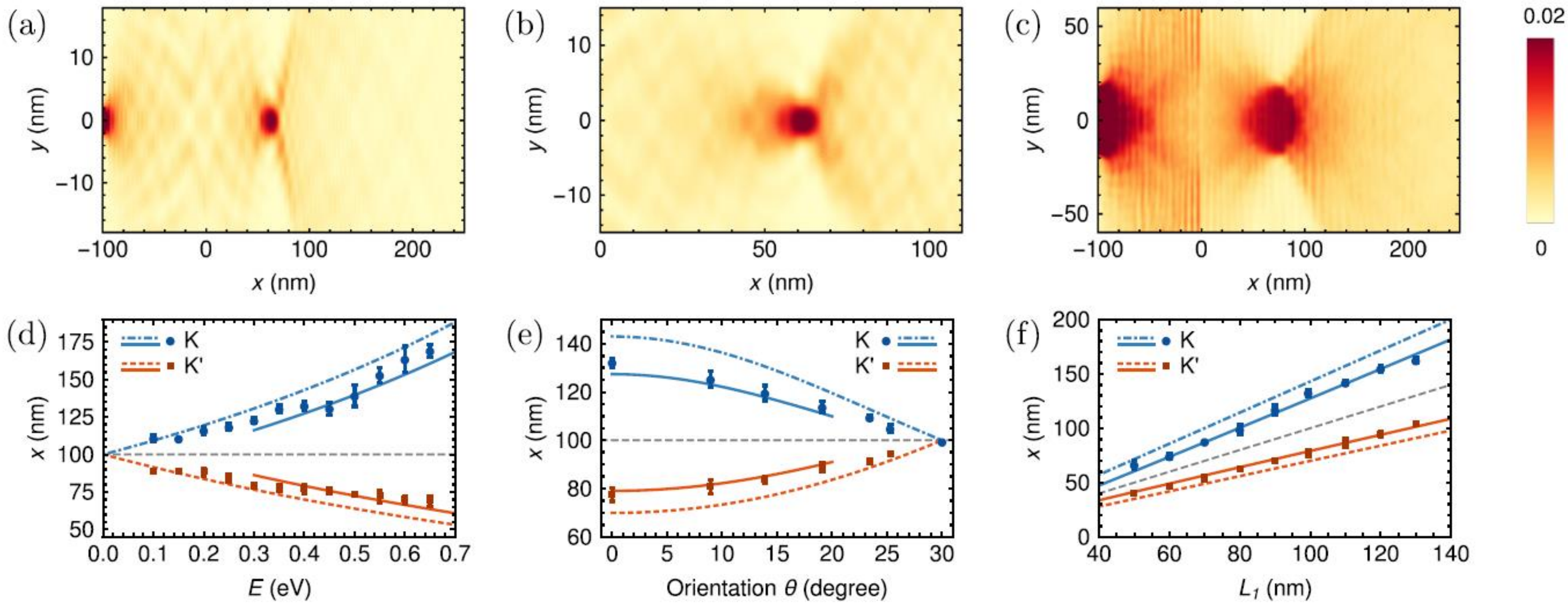

FIG. 2. (a)–(c) Results of the tight-binding simulations with $L_1 = 100$ nm. The density $|\Psi_{\mathrm{av},\alpha}|^2$ is averaged over sublattices and summed over lead modes in valley α. (a) K' valley, $E = 0.6$ eV, $U_0 = 2E$, $W_i = 7.5$ nm; (b) K' valley, $E = 0.6$ eV, $U_0 = 1.18$ eV, $W_i = 7.5$ nm; cf. the classical trajectories in Fig. 1(e); (c) K' valley, $E = 0.4$ eV, $U_0 = 2E$, $W_i = 40$ nm. (d)–(f) Position, on the x axis, of the caustic (dashed and dashed-dotted lines), semiclassical maximum (solid lines), and simulated maximum (symbols) for varying energy E, lattice orientation θ, and L_1. The dashed gray lines indicate the Dirac result. The parameters equal (e),(f) $E = 0.4$ eV, (d),(f) $\theta = 0$, (d),(e) $L_1 = 100$ nm, (d),(f) $W_i = 40$ nm, and (e) $W_i = 50$ nm. In all cases $U_0 = 2E$.

Semiclassical (Pearcey) approximation works very well; qualitatively, the splitting can be understood just from classical trajectories

Two-dimensional case

Electronic optics in graphene in the semiclassical approximation

K.J.A. Reijnders [a,*], D.S. Minenkov [b], M.I. Katsnelson [a], S.Yu. Dobrokhotov [b,c]

Annals of Physics 397 (2018) 65–135

$$\hat{H}_\alpha \Psi_\alpha = E \Psi_\alpha, \qquad \Psi_\alpha = \begin{pmatrix} \psi_1 \\ \psi_2 \end{pmatrix}$$

$$\hat{H}_\alpha = \begin{pmatrix} U(x) + m(x) & \hat{p}_1 + i\alpha \hat{p}_2 \\ \hat{p}_1 - i\alpha \hat{p}_2 & U(x) - m(x) \end{pmatrix}$$

$$x = (x_1, x_2)$$

$\alpha = -1$ for the K-valley and $\alpha = +1$ for the K'-valley

Only above-barrier case is considered; even this is quite demanding, tunneling problem is extremely difficult

$(U(x) - E)^2 - m(x)^2 > 0$ for all x

Operators and symbols

$f(x,p)$ is a classical observable dependent on coordinates and momenta

It can be considered as a symbol of (pseudodifferential) operator $Op_t(f)$

$$Op_t(f)u(x) = \frac{1}{(2\pi h)^n}\int e^{i\langle p, x-y\rangle/h} f\big((1-t)x + ty, p\big)u(y)\,dy\,dp$$

Example:

$f(x,p) = \langle x,p\rangle$ $\quad$ $Op_0(\langle x,p\rangle)u(x) = -ih\langle x, \partial u(x)/\partial x\rangle$

$Op_0(\langle x,p\rangle) = \langle x,\hat{p}\rangle$ but $Op_{1/2}(\langle x,p\rangle) = \frac{1}{2}(\langle x,\hat{p}\rangle + \langle \hat{p},x\rangle)$

Operators and symbols II

$$f(x,p)=\sum_\beta f_\beta(x)p^\beta$$

$$p^\beta=\prod_i p_i^{\beta_i}$$

$$Op_0(f)=\sum_\beta f_\beta(x)\hat{p}^\beta$$

Oppositely, from operator to symbol: $a^{(t)}=\sigma_t(\hat{a})$ $\hat{a}=Op_t(a^{(t)})$

$$a^{(0)}(x,p,h)=\sigma_0(\hat{a})=e^{-i\langle p,x\rangle/h}(\hat{a}e^{i\langle p,x\rangle/h})$$

$$a^{(t')}(x,p,h)=\exp\left(ih(t'-t)\left\langle\frac{\partial}{\partial x},\frac{\partial}{\partial p}\right\rangle\right)a^{(t)}(x,p,h)$$

Example:

$$\hat{a}=\frac{1}{2}(\langle x,\hat{p}\rangle+\langle\hat{p},x\rangle)$$

$$a^{(0)}=\langle x,p\rangle-inh/2$$

$$a^{(1/2)}=\langle x,p\rangle$$

Operators and symbols III

Standard quantization: t = 0

$$\hat{a}\, u(x) = \mathrm{Op}_0(a)u(x) = a(x,\hat{p},h)u(x) = \mathcal{F}^{-1}_{p\to x}a(x,p,h)\mathcal{F}_{y\to p}u(y)$$

Weyl quantization: t = 1/2

$$\begin{aligned}\hat{a}\, u(x) &= \mathrm{Op}_{1/2}(a)u(x) = a^W(x,\hat{p},h)u(x)\\ &= \frac{1}{(2\pi h)^2}\int e^{i\langle p,x-y\rangle/h}a\left(\frac{x+y}{2},p,h\right)u(y)dydp\end{aligned}$$

Symbols are extremely convenient for expansion in h

$$a^{(t)}(x,p,h) = \sum_j a_j^{(t)}(x,p)h^j$$

Semiclassics for matrix Hamiltonians

Belov *et al.*, J Eng Math 55, 183 (2006); Littlejohn, Flynn, Phys Rev A 44, 5239 (1991)

$\hat{H}\Psi = E\Psi$, where $\hat{H}$ is an $n \times n$ matrix

Ψ is an n-dimensional vector

We try the solution $\Psi(x) = \hat{\chi}\,\psi(x)$

ψ is an effective scalar wavefunction

$\hat{L}\psi = E\psi$ $\hat{L}$ plays the role of the scalar Hamiltonian

Operator equation to solve $\hat{H}\hat{\chi} - \hat{\chi}\hat{L} = 0$

Matrix Hamiltonians II

In zeroth order in *h*

$$H_0(x,p)\chi_0(x,p) = L_0(x,p)\chi_0(x,p)$$

which means that the principal symbols L_0 and χ_0 are the eigenvalues and eigenvectors, respectively, of the principal symbol of the matrix Hamiltonian $\hat{H}$. Note that H_0 is an $n \times n$ matrix and χ_0 is an n-dimensional vector.

First order in *h*

$$L_1 = \underbrace{-i\chi_0^\dagger\{\chi_0, L_0\}}_{\text{Berry part } L_{1B}} \underbrace{-\frac{i}{2}\sum_{j,k}(H_{jk} - L_0\delta_{jk})\{\chi_{0,j}^*, \chi_{0,k}\}}_{\text{Additional part } L_{1A}}$$

2D Dirac Hamiltonian

$$L_0^\pm(\mathbf{x},\mathbf{p}) = U(\mathbf{x}) \pm \sqrt{p^2 + m^2(\mathbf{x})}$$

$$L_{1,\alpha}^\pm(\mathbf{x},\mathbf{p}) = \frac{\alpha}{2\sqrt{p^2+m^2}(\sqrt{p^2+m^2} \mp m)}\left(p_2\frac{\partial(U+m)}{\partial x_1} - p_1\frac{\partial(U+m)}{\partial x_2}\right)$$

Semiclassical equations of motion

$$\frac{dx_j}{dt} = \frac{\partial L_0}{\partial p_j} + h\frac{\partial L^W_{1,A}}{\partial p_j} + h\sum_k (\Omega_{pp})_{jk}\frac{\partial L_0}{\partial x_k} - h\sum_k (\Omega_{px})_{jk}\frac{\partial L_0}{\partial p_k},$$

$$\frac{dp_j}{dt} = -\frac{\partial L_0}{\partial x_j} - h\frac{\partial L^W_{1,A}}{\partial x_j} - h\sum_k (\Omega_{xp})_{jk}\frac{\partial L_0}{\partial x_k} + h\sum_k (\Omega_{xx})_{jk}\frac{\partial L_0}{\partial p_k}.$$

$$(\Omega_{xp})_{jk} = i\left(\frac{\partial \chi_0^\dagger}{\partial x_j}\frac{\partial \chi_0}{\partial p_k} - \frac{\partial \chi_0^\dagger}{\partial p_k}\frac{\partial \chi_0}{\partial x_j}\right)$$

is the Berry curvature (This derivation: Littlejohn & Flynn 1991)

As used in the theory of topological matter

Xiao, Chang & Niu, RMP 82, 1959 (2010)

Scattering by potential bump or well

$$U(x) = -U_0 \exp(-x^2/L^2)$$

$$\tilde{U}(\tilde{x}) = -\tilde{U}_0 \exp(-\tilde{x}^2)$$

Classical trajectories

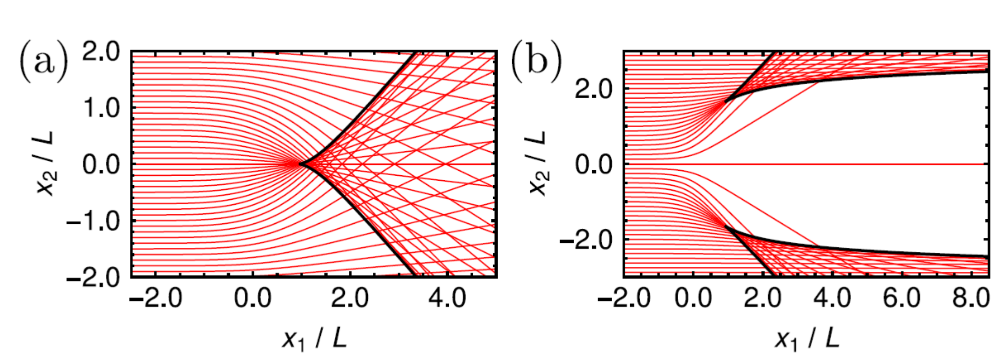

$\tilde{U}_0 = \frac{1}{2}$ and $\tilde{m}(\tilde{x}) = 0$

$\tilde{U}_0 = -\frac{1}{2}$ and $\tilde{m}(\tilde{x}) = 0$

Semiclassical solution

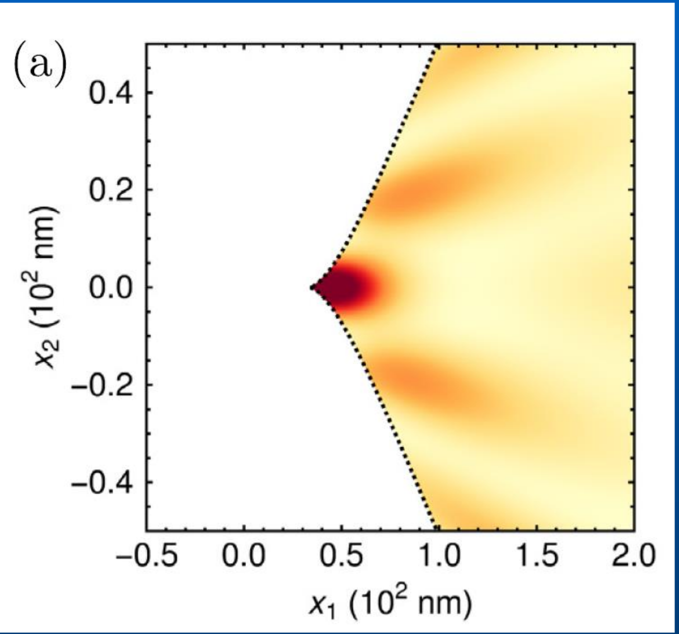

$\|\Psi\|^2$ for $E = 200$ meV, $U_0 = 100$ meV and $L = 35.5$ nm

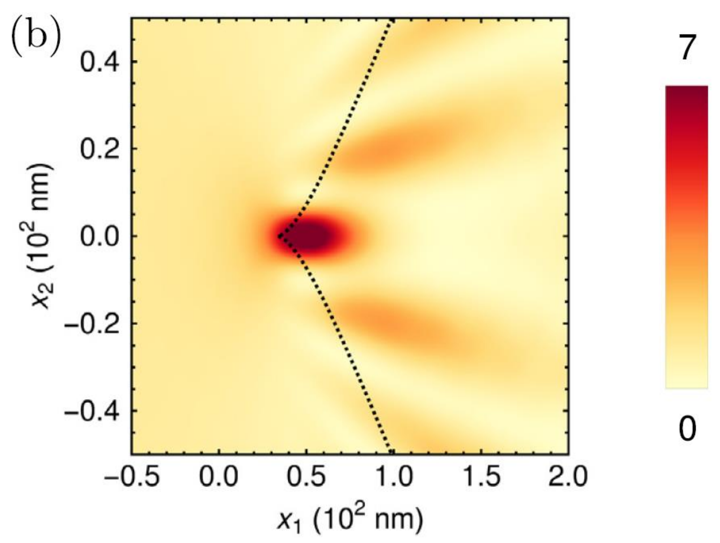

Exact numerical solution at the lattice

The role of semiclassical phase

$$L_0(x,p) = \sqrt{p^2 + m^2(x)} + U(x) = E$$

Can be rewritten as $\mathcal{L}_0(x,p) \equiv C(x)|p| = 1, \quad \text{where } C(x) = \frac{1}{\sqrt{(E - U(x))^2 - m^2(x)}}$

(a new "Hamiltonian", new "energy" = 1)

When we set $U(x) = E - \sqrt{E^2 + m^2(x)}$ $\quad C(x) = \frac{1}{\sqrt{(U(x) - E)^2 - m^2(x)}} = \frac{1}{E}$

and classically there is no effect on electron motion.

Only semiclassical phase matters in this situation

The role of semiclassical phase II

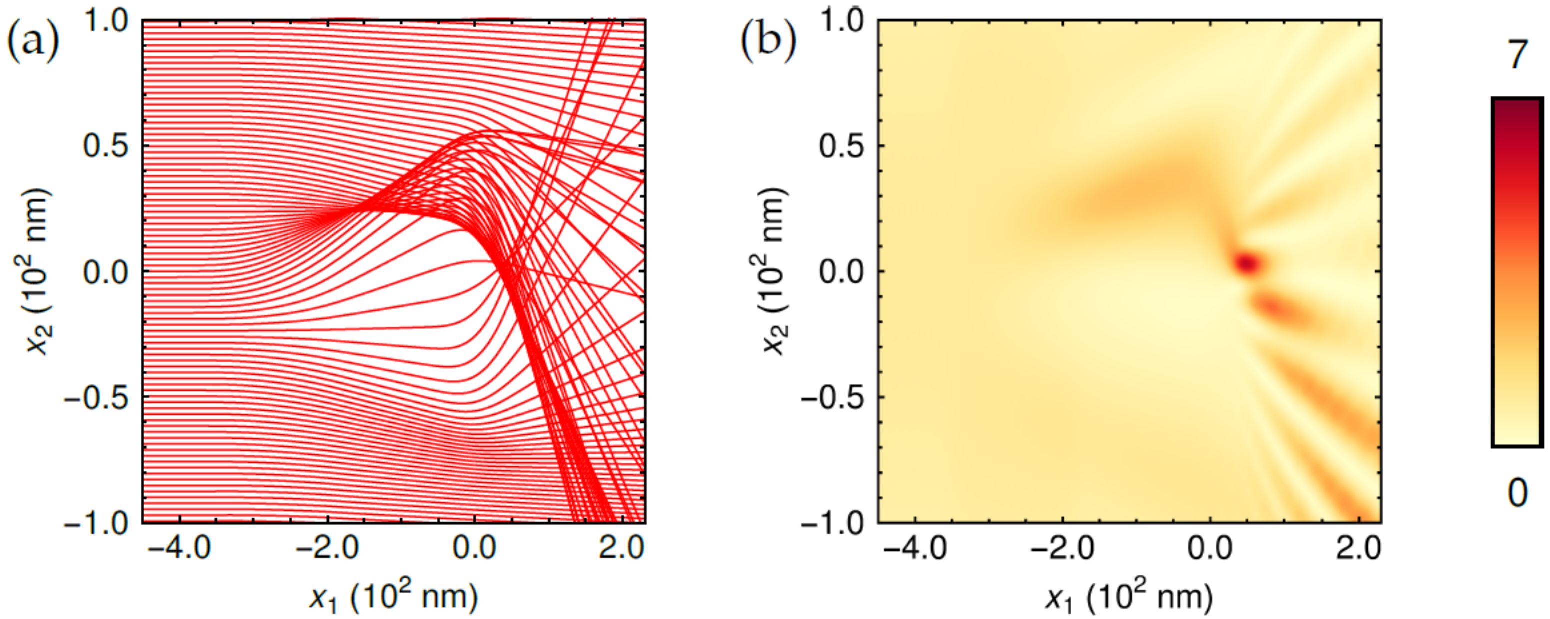

Figure 6.9: (a) Trajectories for an electron in the K′ valley, computed using the modified equations of motion (6.27). (b) Result of a tight-binding calculation for a zigzag sample with a width of 4000 $a_{CC} \approx 568$ nm. To produce these figures, we used the same parameters as in figure 6.8.

Bilayer graphene – TB description

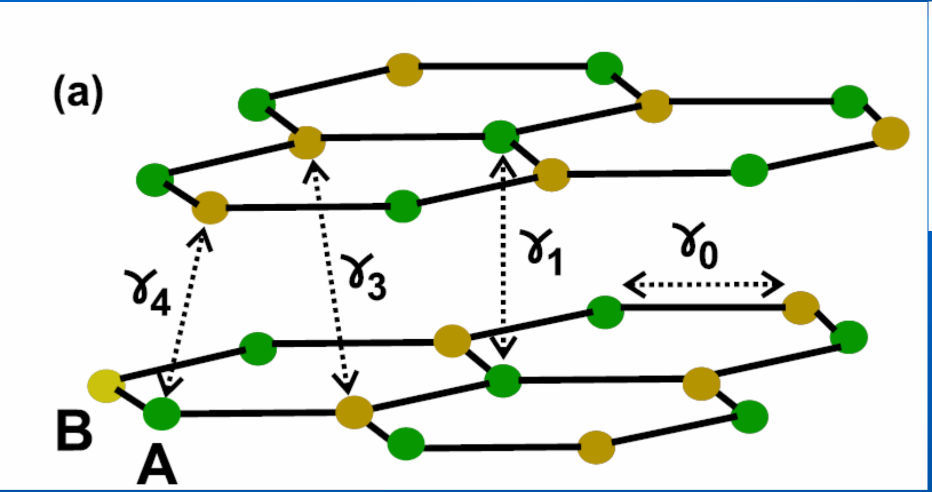

$$H = \begin{pmatrix} 0 & -(p_x - ip_y)^2/2m \\ -(p_x + ip_y)^2/2m & 0 \end{pmatrix}$$

$$m^* \approx 0.028 m_e$$

(neglecting γ_3)

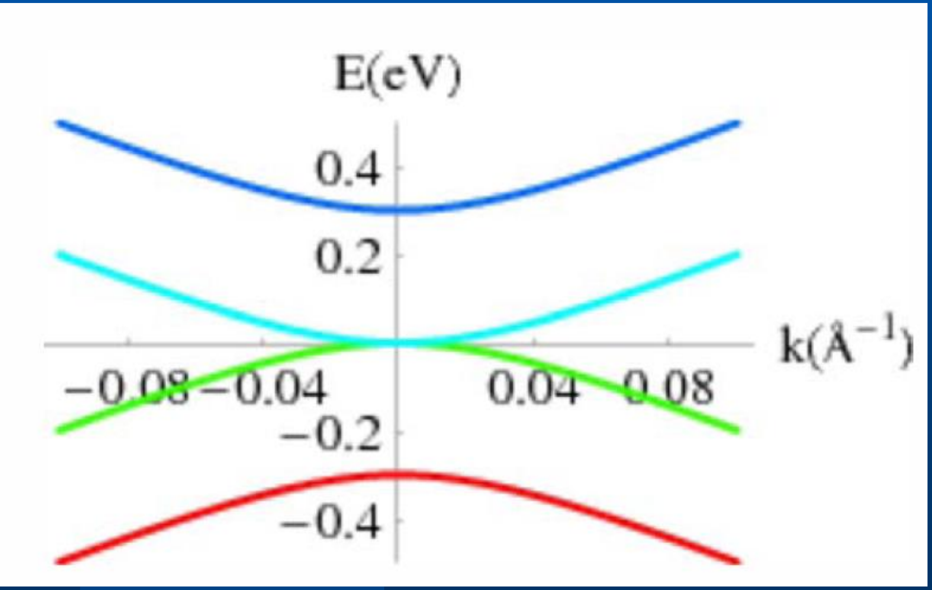

Gapless, parabolic

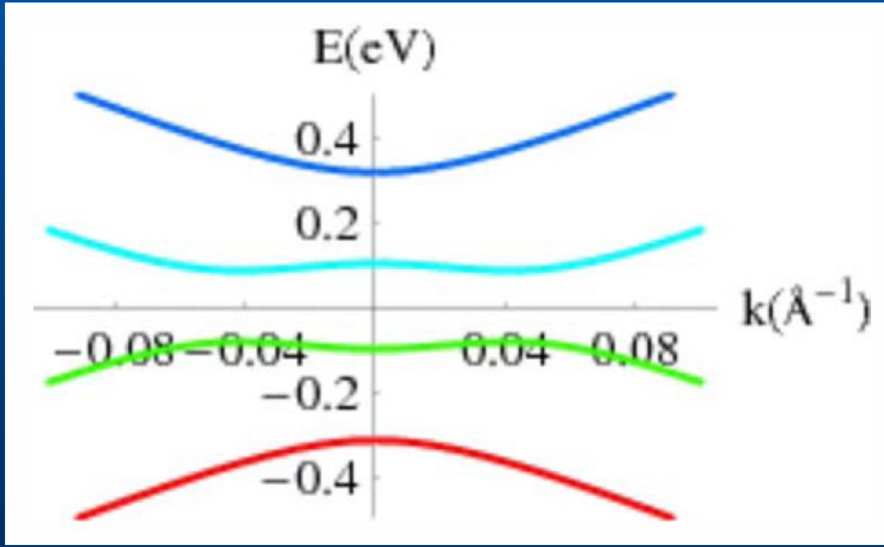

Electric field perp. layers

Bilayer graphene II

Trigonal warping, many-body effects and spectrum reconstruction at small energies

Single-particle Hamiltonian:

$$\hat{H}_{\mathrm{K}} = \begin{pmatrix} 0 & \frac{\left(\hat{p}_x - i\hat{p}_y\right)^2}{2m^*} + \frac{3\gamma_3 a}{\hbar}\left(\hat{p}_x + i\hat{p}_y\right) \\ \frac{\left(\hat{p}_x + i\hat{p}_y\right)^2}{2m^*} + \frac{3\gamma_3 a}{\hbar}\left(\hat{p}_x - i\hat{p}_y\right) & 0 \end{pmatrix}$$

Interaction-Driven Spectrum Reconstruction in Bilayer Graphene

A. S. Mayorov,[1] D. C. Elias,[1] M. Mucha-Kruczynski,[2] R. V. Gorbachev,[3] T. Tudorovskiy,[4] A. Zhukov,[3] S. V. Morozov,[5] M. I. Katsnelson,[4] V. I. Fal'ko,[2] A. K. Geim,[3] K. S. Novoselov[1*]

12 AUGUST 2011 VOL 333 SCIENCE

Chiral tunneling - bilayer

Problem: graphene transistor can hardly be locked!

Possible solution: use bilayer graphene: chiral fermions with parabolic spectrum – no analogue in particle physics!

Transmission for bilayer; parameters are the same as for previous slide

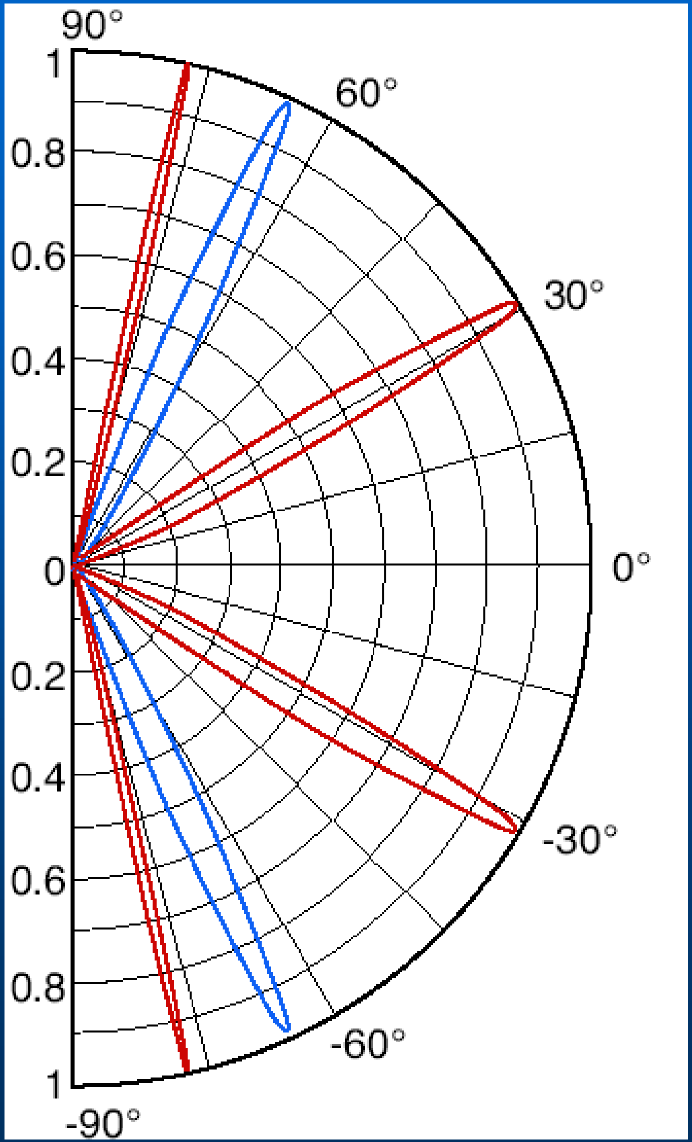

Chiral tunneling – bilayer II

Kleptsyn, Okunev, Schurov, Zubov & MIK, PRB **92**, 165407 (2015)

For symmetric potential V(x)=V(-x): one real equation for magic angles but not necessarily real solutions

Magic angles are not protected

Example: fast-oscillating potential

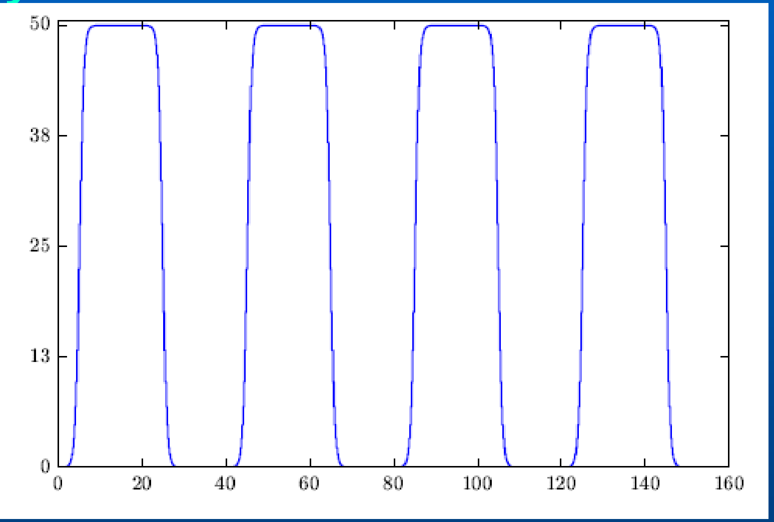

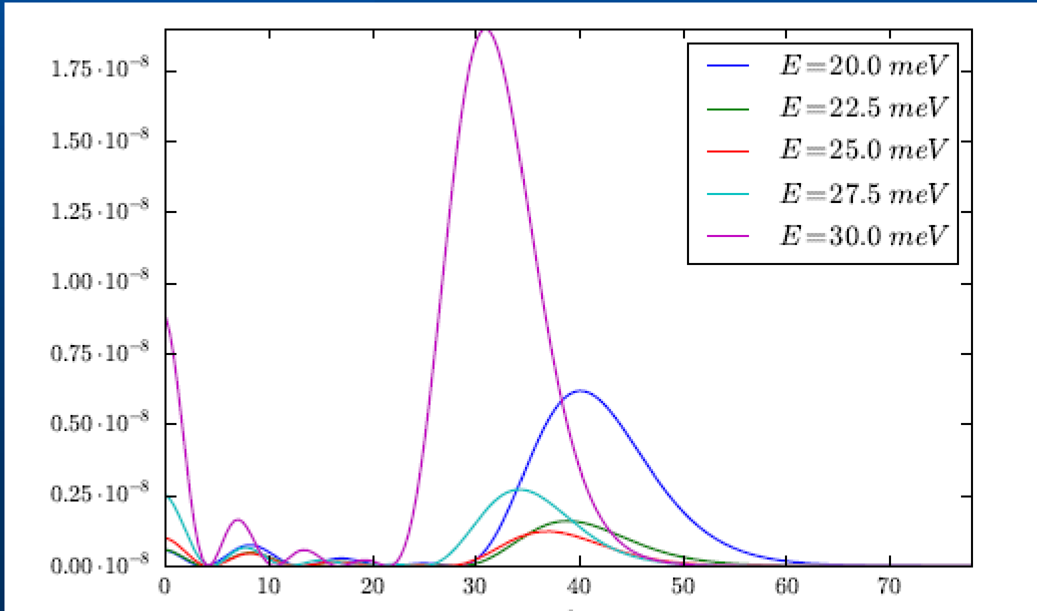

Very small transmission probability

From analysis of ODE to graphene transistor?!

Conclusions

Semiclassical approximation is not only a qualitative tool to understand numerical data (which is very important by itself) but also frequently gives you quite accurate quantitative results

Still open questions:

- Tunneling in more than one dimension;
- Tunneling in bilayer graphene